1

Combustion Synthesis of Nitrides for Development of Ceramic Materials of New Generation

Inna P. Borovinskaya, Vazgen E. Loryan, and Vladimir V. Zakorzhevsky

1.1
Introduction

Metal and nonmetal nitrides are remarkable compounds characterized by a great number of valuable and interesting properties such as high chemical stability in different aggressive media, heat resistance, ability to transition to superconducting state, excellent semiconducting and dielectric characteristics, high hardness which is sometimes close to that of diamond, and so on. Nitride ceramics is widely applied in various industries, for example, electronics, ferrous and nonferrous metallurgy, aerospace, and nuclear power engineering. It is not surprising that since the time when the first nitrides were obtained, active investigations have been carried out to understand the character of nitrides, their behavior and relationship of their properties with peculiarities of their structure, and chemical bonds. The increasing requirements to the quality and operation properties of nitride ceramics make the researchers improve the available synthesis methods and develop new efficient technologies. Self-propagating high-temperature synthesis (SHS) based on combustion processes [1–6] is one of the leading methods of investigation of theory and practice, structure and phase formation of nitrides in the combustion mode, development of new variations of synthesis and technology of nitrides and composite materials thereof, and items and parts based on nitride ceramics for various application purposes. By this time, a lot of articles have been published in all the spheres of the exploration. Their level is constantly being increased. In this chapter, we try to analyze the investigation results of regularities and mechanism of metal and nonmetal combustion in nitrogen as well as structure and phase formation of nitrides, which appear to be less known or unpublished in literature. Besides, we demonstrate some scientific and practical achievements in development of SHS powder technology of the most important nitrides, direct synthesis of SHS materials and items based on nitride ceramics, and some examples of their practical application. The presented information employs the experimental work carried out at the Institute of Structural Macrokinetics and Materials Science of the Russian Academy of Sciences.

1.2

Peculiarities of Phase and Structure Formation of Metal and Nonmetal Nitrides in Combustion Mode

The first regularities of nitride structure were established by Hagg [7]. He gave the definition of the primary structures in which nonmetal atoms penetrated into the metal crystal lattice and called them "penetration structures." Face-centered cubic, volume-centered cubic, hexagonal compact, and hexagonal simple types of lattice are the most common for the penetration structures. According to Hagg, transition-metal nitrides (metal-like nitrides) are typical penetration structures. The penetration phases are often considered as heterodesmic compounds with complex superimposition of covalent, metal, and ionic bonds. Many scientists think that the combination of the bonds is the main reason of the extraordinary behavior and unique properties of nitrides. So-called nonmetal nitrides, for example, BN, Si_3N_4, AlN, and so on, are mainly characterized by covalent bonds and appear to be actual chemical compounds. The works in SHS studied the regularities and mechanism of phase and structure formation of both types of nitrides: metal-like and nonmetal.

1.2.1

Systems of Transition Metal of the IV–V Groups of the Periodic Table with Nitrogen

Single-phase solid solutions of nitrogen in metals are "lower" phases of the systems of metal (IV–V groups)-nitrogen formed directly in the course of SHS. The conditions and mechanism of their formation have been extensively studied in combustion of porous titanium and zirconium samples at gaseous nitrogen pressures of 0.1 up to 500 MPa [8–10]. Theoretical consideration of the possibility of combustion between metals and nonmetals forming merely solid solutions was carried out in [11]. The systems of $Zr + N_2$ and $Ti + N_2$ are the most highly exothermic. Homogeneity regions of α-solid solutions of nitrogen in these metals are fairly large and attain compositions of $ZrN_{0.33}$ and $TiN_{0.27}$. Thermodynamic calculations and experiments have shown that the SHS process in $Zr + N_2$ and $Ti + N_2$ systems is possible to occur at the expense of solid solution formation. The dependence of the calculated adiabatic combustion temperature in $Zr + N_2$ system on nitrogen content in the homogeneity region of the solid solution is given in Figure 1.1. The combustion temperatures are seen to be high. A necessary condition for the formation of single-phase solid solution of nitrogen in metals is the arrest of the reaction at the stage of the solid solution formation. The further nitriding of the solid solution can be ceased in several ways. The most common ones are the sample quenching in liquid argon and sharp gas drop immediately after the combustion front passage [1, 8]. The efficient way is also to create the conditions when after-burning (bulk after-nitriding of the samples heated in the
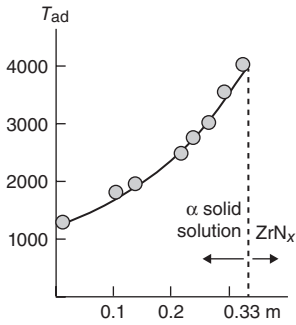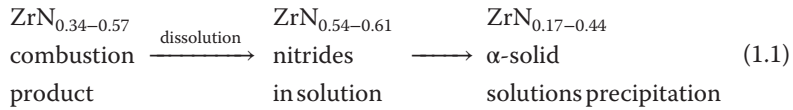
Figure 1.1   Combustion temperature versus solid solution composition. m – N_2 content (relative units).

combustion front) is unlikely to happen [1, 8]. In $Zr + N_2$ and $Ti + N_2$ systems, such unfavorable conditions are formed spontaneously since the sample under combustion often becomes sintered or molten (especially at nitrogen pressure of >3 MPa), and there is no access for the gas into the combustion zone. Other techniques eliminating the after-burning can be: confining the sample's lateral surface in a gas-tight jacket, implementing the combustion process in the mixture of metals with nitrides in a pure surface combustion mode, which plays the role of a "chemical furnace" to facilitate the product homogenization or dissolving nitrogen with inert gas, for example, argon [8, 12]. Combustion of the mixtures of metals with nitrides in the "chemical furnace" mode is analogous to the furnace synthesis of nitrogen solid solutions in metals by homogenization. American scientist observed the combustion wave propagation due to the formation of TiN_{1-x} thin layer with the formation of nitrogen solid solution in the quenched combustion products using X-ray analysis and scanning electron microscope (SEM) [13].

An important achievement in the studies of the direct combustion synthesis of solid solutions was the production of compositions with minimum nitrogen content ($MeN_{0.13} - MeN_{0.22}$) and synthesis of single-phase oversaturated solid solutions of $MeN_{0.34} - MeN_{0.45}$ with nitrogen content exceeding the value known from literature. This fact initiated the hypothesis of nitride formation in the combustion mode by means of saturating metal with nitrogen along with forming oversaturated solid solutions which are then decomposed to form a solid solution of a lower composition and nonstoichiometric nitride MeN_x in contrast to commonly accepted mechanism of the reaction diffusion through the product film. In this case, the combustion rate is determined by the rate of the nonmetal dissolution in metal. At this stage, the major heat release takes place. This concept was presented in [14].

The chemical and phase analyses of the compositions from $ZrN_{0.34}$ to $ZrN_{0.57}$ prove that the combustion products are oversaturated solid solutions. They decompose when annealed or dissolved in some specific liquids to solid solutions

of a lower composition and nonstoichiometric nitrides.

$$
\begin{array}{ccc}
\text{ZrN}_{0.34-0.57} & \text{ZrN}_{0.54-0.61} & \text{ZrN}_{0.17-0.44} \\
\text{combustion} \xrightarrow{\text{dissolution}} & \text{nitrides} \longrightarrow & \text{α-solid} \\
\text{product} & \text{in solution} & \text{solutions precipitation}
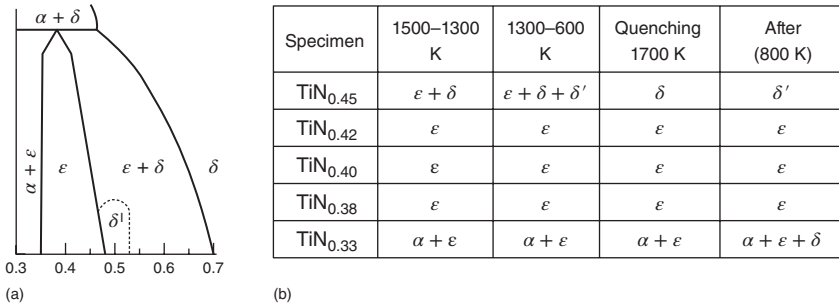\end{array} \qquad (1.1)
$$

Metallographic investigations of the sample microstructure prove nitride evolution on the grain boundaries.

Generalizing these concepts for various metal–nonmetal systems, one can assume that the systems with wide regions of homogeneity of solid solutions can burn, under certain conditions, involving the stage of the solid solution saturation without yielding any compounds. The systems with narrow regions of homogeneity of solid solutions under specific conditions (reactive mass melting, high pressures) can also produce solid solutions when burning with their subsequent decomposition or crystallization. As to Me–N systems with complex state diagrams (e.g., Ta–N, Nb–N) which comprise solid solutions with narrow regions of homogeneity, single-phase solid solutions in these systems are also formed during the combustion. However, it is difficult to isolate them. They can only be observed in the quenched products in the layers adjacent to the combustion front, so-called warming-up zones [15, 16].

Examples of interaction including nonmetal dissolving in metals in solid–solid systems were described by Vidavsky [17] for Zr–C systems, and by Itin and Bratchykov [18] for SHS intermetallics particularly for Ti–Co system. Aleksandrov and Boldyrev [19] and Holt with coworkers [20] performed direct observation of the dissolving stage during SHS product formation in Ni–Al and Ti–C systems by measuring the phase structure of the combustion wave by means of synchrotron radiation. Shteinberg with coworkers obtained unique results on carbon dissolving in titanium under thermal explosion. The authors thoroughly investigated the mechanism of this process and regularities of structure formation [21].

One of the interesting examples of chemical stages in the SHS processes with lower phase formation is the occurrence of the metastable phase of ε-Ti$_2$N during titanium combustion in gaseous nitrogen. The combustion process in this system was studied in our work [22, 23] as well as in the works carried out by Japanese scientists Hirao *et al.* [24] and American colleagues Munir *et al.* [25].

According to literature data, the phase of ε-Ti$_2$N is unstable and starts decomposing at temperatures exceeding $1000-1100\,^\circ$C. We first produced this phase when decomposing oversaturated solid solutions of nitrogen in titanium of TiN$_{0.33}$–TiN$_{0.42}$ composition. Besides, ε-Ti$_2$N phase was discovered in the quenched products of titanium combustion in nitrogen at $P = 300-450$ MPa. The following studies by Karimov and Em with coworkers [26, 27] dealt with combustion products of Ti–N system. They used neutron diffractometer ($\lambda = 1.08$ Å) which was installed at the thermal column of a nuclear reactor. In their experiments, the specimens were undergoing heat treatment (homogenizing annealing) in the temperature range of $1500-1300$ K with quenching from 1700 K and

Specimen	1500–1300 K	1300–600 K	Quenching 1700 K	After (800 K)
$TiN_{0.45}$	$\varepsilon + \delta$	$\varepsilon + \delta + \delta'$	δ	δ'
$TiN_{0.42}$	ε	ε	ε	ε
$TiN_{0.40}$	ε	ε	ε	ε
$TiN_{0.38}$	ε	ε	ε	ε
$TiN_{0.33}$	$\alpha + \varepsilon$	$\alpha + \varepsilon$	$\alpha + \varepsilon$	$\alpha + \varepsilon + \delta$

(a)   (b)

Figure 1.2 Neutron diffraction study (a, b): (a) state diagram of Ti−N system and (b) phase composition of products after thermal treatment.

subsequent annealing of the products after quenching at 800 K. ε-Phase was found to be formed in the concentration range of $0.38 \leq N/Ti \leq 0.42$. The ε-Ti_2N_{1-x} phase ($0.24 \geq x \geq 0.16$) is characterized by lower nitrogen content as compared to that of stoichiometric compound Ti_2N. The ordered tetragonal phase δ'-Ti_2N was found to be formed at 800 K on the base of metastable high-temperature cubic δ-phase. Its homogeneity region is in the range of $0 \leq x \leq 0.1$. Based on the obtained data, a more precise diagram of the Ti−N system was suggested. A fragment of this diagram and phase composition of the products after heat treatment are presented in Figure 1.2.

1.2.1.1 Two Threshold Mechanisms of Combustion and Structure Formation

A hypothesis on stepped formation of final SHS products through formation of amorphous substances being primary combustion products was suggested by Merzhanov [28] on the base of experimental studies. It should be noted that certain amorphous phases of some SHS nitrides were isolated and identified in earlier works [8]. Most of the nitrides synthesized at optimum combustion terms are polycrystals. Usually, they are in equilibrium state and have distinct, narrow characteristic peaks in X-ray patterns. Many of them can be considered as typical examples of equilibrium compounds. Nevertheless, under special or nonoptimum synthesis conditions and, particularly, during cooling (natural or forced quenching), the formation of nonequilibrium products with blurred and broadened lines in X-ray patterns is observed. It proves the appearance of amorphous phases, which later acquire a certain crystalline structure depending on the process conditions (combustion and cooling temperature and rate, presence of crystallizers, etc.). The formation of amorphous phases was frequently observed when nonmetals (boron, silicon, and phosphorus) were burnt in high-pressure nitrogen atmosphere ($P_{N_2} = 300 - 800$ MPa). Amorphous phases can be crystallized during heating or long exposure to room temperature. The chemical analysis of the amorphous products reveals that their composition corresponds to that of stoichiometric nitrides. However, in some cases, the unknown phases were obtained, for example, pink-brownish boron nitride of

$BN_{0.75}$ composition. After heating or extended exposure to room temperature, amorphous stoichiometric compounds, as mentioned before, are crystallized, retaining their chemical composition. When synthesizing boron nitride from boron anhydride (SHS with a reduction stage), Mamyan [29] also observed the formation of amorphous SHS products. Amosov [30] obtained amorphous products when synthesizing silicon nitride in azides presence. In our experiments, amorphous silicon nitride was produced when silicon powder was burnt in gaseous nitrogen in the presence of ammonium chloride. In these reactions, amorphous silicon diimide was identified as an intermediate product, which is known to be a network polymer. This intermediate compound is a source of SHS nitride with a unique particle structure in the form of fibers. Silicon nitride powders with different particle structures (agglomerates and column crystals) were obtained at various combustion terms. The mechanism of their formation in the SHS mode was thoroughly studied in [31–34].

Later on, Merzhanov [28] suggested the conception of structure formation in SHS processes. The starting point was the idea of complete destruction of the phase composition of the initial components during the chemical reaction and formation of a new "primary" microstructure. Two threshold combustion and structure formation mechanisms in SHS processes were defined in connection with characteristic times of combustion t_c and structure formation t_s, Figure 1.3. If $t_s/t_c \ll 1$, the equilibrium mechanism of structure formation takes place. In this case, the SHS reaction proceeds by the mechanism of the reactive diffusion
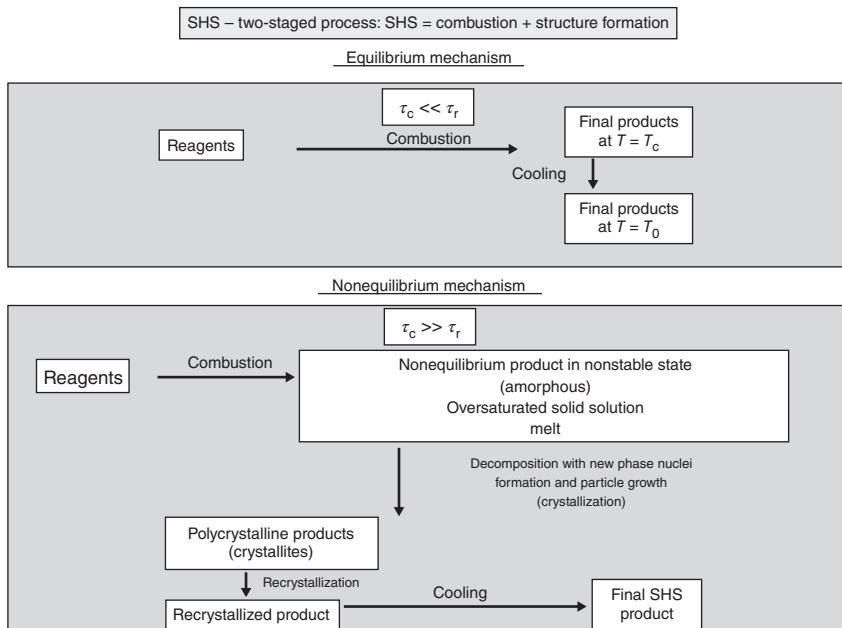

Figure 1.3 Two threshold mechanisms of final product formation in SHS processes.

and yields the equilibrium product, which does not undergo any structural transformations. Structure formation of the final product influences the combustion front and chemical transformation velocity. The equilibrium mechanism taking its name from the conception by Khaikin–Aldushin–Merzhanov is preferable for slow-burning systems. If $t_s/t_c \gg 1$, the nonequilibrium mechanism of structure formation takes place. During the reaction, the products appear to be in metastable state: oversaturated solid solutions, amorphous phases, and melts. After chemical reactions in these products, phase structural transformations occur far behind the combustion front. These processes do not affect the reaction and combustion front rates. We can change the ratio of the characteristic times of combustion product structure formation t_s and cooling t_{rel} and thereby regulate the completeness of structure formation and obtain either nonequilibrium products ($t_{rel}/t_s \ll 1$) or equilibrium ones ($t_{rel}/t_s \gg 1$). At the nonequilibrium mechanism named after Borovinskaya, local equilibrium state of the substance is absent in the combustion wave, and it is preferable for fast-burning systems.

Nowadays, the subject of structure formation during SHS reactions is being developed by means of novel methods used in structural macrokinetics: X-ray microanalysis, optical spectroscopy, Auger spectroscopy, electronic microscopes, and physical and mathematical modeling. Of great importance in investigation of structure formation in SHS is local dynamic X-ray spectrum analysis using diffractometer with a special detector [35]. Processing of the diffraction patterns allows plotting the kinetic curves of phase composition changes in the combustion wave and getting information on chemical and phase transformations. The mentioned method is used to study formation mechanism of specific products and intermediate phases from the initial green mixtures to final products in the systems of solid–solid, but there are also some works demonstrating the combustion product formation in the solid–gas systems.

1.2.1.2 Structural and Morphological Peculiarities of Silicon, Boron, and Aluminum Nitrides – Nanosized Powders

Many experimental results proving the formation of various nonequilibrium products and investigation of synthesis peculiarities of nitrides formed under nonequilibrium terms (high synthesis velocities and fast crystallization of combustion products) give the go-ahead to the SHS processes in such an actual field as nano-industry and throw a sidelight upon the mechanism of nanodispersed particle formation. The conception of SHS of nanomaterials can be presented using the scheme suggested by Merzhanov, Figure 1.4 [36]. According to the figure, nanoparticles are formed and then grown under the nonequilibrium terms of SHS processes. The size and amount of nanoparticles depend on the combustion temperature and on the cooling time as well. There are some nanoparticles in the samples, which are cooled naturally. It is necessary to quench them in order to increase the nanoparticle amount. The possibility of nanoproduct formation at combustion of various SHS systems (solid–solid, solid–gas, gas-phase SHS, etc.) was considered in the work by Sytchev and Merzhanov [37]. In our days, we have obtained a lot of powder SHS compounds with nanodispersed particles, and even
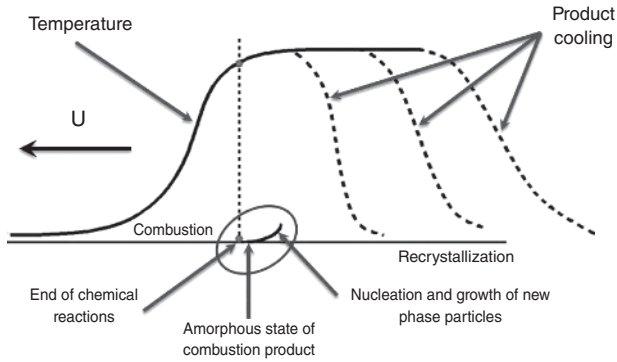
Figure 1.4 SHS product structure formation in combustion wave.

tubular nanostructures as well as nanostructured materials. Figure 1.5 demonstrates some of SHS nanopowders synthesized by combustion. The experimental investigation on the mechanism and regularities of nanoparticle formation in refractory inorganic compounds and the methods of their separation show that the following approaches are the most efficient: transfer of the combustion process to the gas-phase mode using gasifying additives or evaporation of solid reagents, fast crystallization of combustion products from melts or gas phase, and chemical dispersion of agglomerated combustion products in special liquids. Specific terms of synthesis and separation of nanodispersed powders shown in Figure 1.5 are described in many original works. This chapter suggests discussing such an
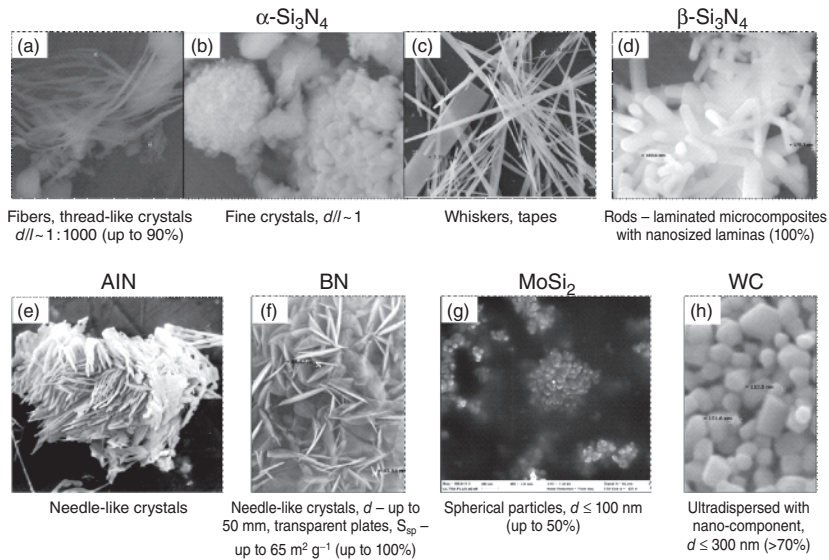
Figure 1.5 (a–h) Nanosized SHS powders of various classes.

important and interesting characteristic of nanomaterial particles as their crystal morphology. Active assimilation of up-to-date investigation methods of synthesized substances such as optical and electron microscopy, atomic spectrometric methods, dynamic X-ray method, and so on allows widening the conception of the material structure, shape, and particle size and even predicting the material properties. However, in most cases, the particle morphology of compounds synthesized by combustion is only considered as an object of some interest. This chapter suggests considering particle morphology as a "tool" for understanding structure formation mechanism at combustion processes. This approach is based on the fact that morphological characteristics can define practical application of a definite material [38]. Therefore, it is more important to study the morphology of a substance than to demonstrate it as an additional approach for understanding the processes occurring during the synthesis. It should be pointed out that the conventional synthesis methods (hydrothermal, gas-phase, melted, etc.) successfully use a morphological variety of some compounds to determine the fields of their application. When studying morphological peculiarities of nitrides and their connection with combustion terms, we used nonmetals nitrides: Si_3N_4, AlN, BN, SiAlONs, and AlONs, as they are characterized by a great variety of forms in comparison with metal nitrides. So-called condensation synthesis was used for obtaining nanosized particles [39]. This method is not well studied and is rather seldom used in SHS. It is based on evaporation of a solid reagent in nitrogen. Also, we applied gas-phase synthesis with gasifying additives and fast-product crystallization from flux melts. Separation of the product was carried out by means of "chemical dispersion."

Silicon Nitride   On the basis of the obtained experimental results, we can point out the following important results. Formation of final holohedral crystals of Si_3N_4 can occur with formation of primary so-called skeleton crystals as hollow rods (Figure 1.6a, b) [6, 40]. They are formed under the terms of "starvation" of the forming nitride crystal, for example, in the case of gaseous nitrogen lack, and prove some infiltration difficulties of the gas supply to the combustion front. These "skeleton" rods gather into spheres. It is typical for structures forming under nonequilibrium terms. When typical β-Si_3N_4 rods were synthesized under equilibrium terms of nitriding without any infiltration difficulties, the conventional scheme of crystal formation by the vapor−liquid−crystal mechanism was observed [41]. It included evaporation of the solid reagent, interaction of its vapor with gaseous nitrogen, formation of a drop with the condensation reaction product dissolved in it (in our case it was silicon nitride), and further crystal growth. In the case of infiltration difficulties of nitrogen supply, the crystal framework grows fast only at the edges because of the maximum mass transfer to them. Due to the material lack, the "starving" crystal tries to grow the "skeleton" and absorbs practically the entire nitrogen, which is only able to grow the protruding parts of the crystal under the terms of the fast growth. As a result, internal cavities, holes, channels, or gutters are formed parallel to the edges in the crystal of hexagonal configuration. This system is nonequilibrium
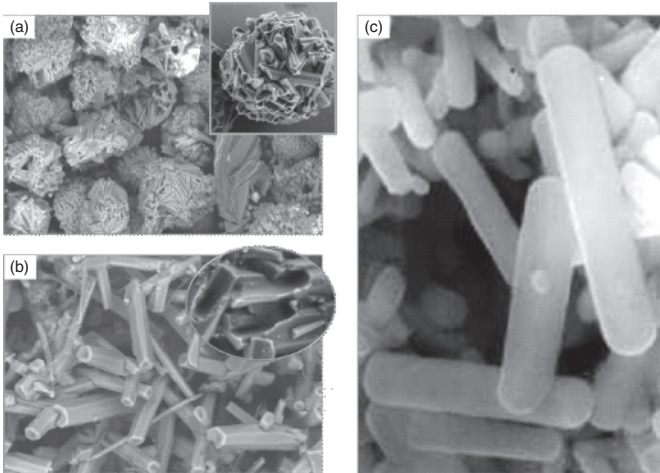
Figure 1.6 β-Si_3N_4 morphology: (a, b) "skeleton" crystals and (c) holohedral crystals.

and energetically unstable, and the most favorable thermodynamic configuration of its existence is a sphere. At mechanical destruction of the sphere, the product disintegrates to separate hollow hexagons (Figure 1.6b). If β-Si_3N_4 rods are treated with alkali, we shall see that the crystal has a laminated structure with a nanosized thickness of the layers, though the crystal itself can be larger than 1 µm. The layers are nitride "flakes" joined to each other by thin layers of melted silicon, which is seen in X-ray patterns while the crystal is treated with alkali.

The total amount of the rods with "skeleton" configuration depends on nitrogen pressure, sample density, and initial nitrogen particle size. The number of the "skeleton" crystals grows with a decrease in nitrogen pressure and an increase in the density of the initial compact samples. Probably, it is connected with the development of infiltration difficulties of gaseous nitrogen supply to the reaction zone. The output of silicon nitride with the morphology of "skeleton" crystals is also increased when the combustion product is hardened by fast drop of gaseous nitrogen pressure after the combustion front propagation or the time of the reactive mass cooling in nitrogen medium is shortened. A decrease in the "skeleton" crystal content in the reactive mass, which is observed in the experiments without nitrogen pressure drop immediately after the combustion front propagation or with an increase in the time of the product cooling in nitrogen medium, proves the ability of β-Si_3N_4 "skeleton" crystals to grow up to standard holohedral rods, Figure 1.6c. It is typical for energetically unstable systems to change in the external terms. In this case, it can be after nitriding of the hot "skeleton" crystals connected with an increase in nitrogen exposure time and better nitrogen supply to incompletely developed products.

Investigation of structure formation mechanism of SiAlONs (solid solutions of $Si_3N_4 - AlN - Al_2O_3$) under the SHS mode with cooling of the reactive mass (quenching of intermediate products) shows that not only individual compounds
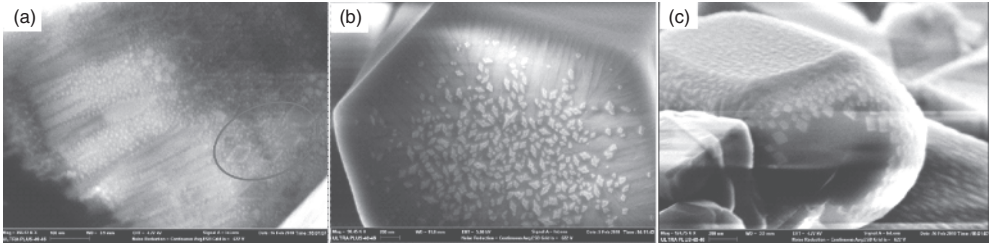
Figure 1.7 Structural transformations of β-SiAlON at thermal treatment in nitrogen, $T \geq 1000\,°C$: (a) crystal internal part and (b, c) second phase on crystal surface.

such as silicon nitride but also more complex systems, for example, solid solutions, can be formed through the stage of skeleton crystal formation. SiAlONs appeared to be interesting compounds for studying structural transformations, chemical and phase composition changes, and variations of properties due to external effect, for example, high-temperature annealing. At $T > 1500\,°C$, β-SiAlON of $Si_4Al_2O_2N_6$ composition transforms to $Si_3Al_3O_3N_5$ with disengagement of some amount of aluminum oxide (Al_2O_3) or AlON ($Al_6O_3N_4$). It can be seen in Figure 1.7a–c that the internal part of the crystal disintegrates into the finest nanofiber bunches with very little spherical formations, which can be considered as nanoparticles. The nanoparticles gather into rhomboid formations on the edges of big crystals. Probably, $Si_3Al_3O_3N_5$ obtained after annealing is supersaturated α-SiAlON containing a large amount of impurity phases of aluminum nitride polytypoids (12H and 21R) and oxide compounds indissoluble in SiAlON crystal lattice.

A rather interesting morphological pattern can be observed in the case of silicon nitride synthesis with crystallization of its particles from the melts of fusing agents, which can be presented by various alkali metal salts. The crystallization mechanism is determined by the existence of the melt, the character of the fusing agent of a simple or complicated composition, including eutectics with a hard reagent, and its behavior during the combustion process. Figure 1.8a demonstrates that initial nitride crystals in NaCl-containing melt have a shape of a sphere. They can be concerned as "antiskeleton" crystals. It can be seen that silicon nitride crystals are formed in the melt in which a great number of crystallization centers appear. Disintegration of the crystal-sphere results in the development of rather complicated branching dendrites (Figure 1.8b,c). According to the well-known mechanism of the dendrite growth of a branching crystal [42], long branches are the first to grow, then some others appear on them until they come into contact with each other and fill the interaxial space. Then the dendrite turns into the crystal (in our case it is β-Si_3N_4) with irregular external faces (Figure 1.8d). Therefore, the dendrite appears to be an intermediate crystal form, which is changed to the acicular one (spherulite). It confirms fast growth of nitride crystals at high velocities of SHS and fast crystallization of combustion products. It is typical for nonequilibrium processes. Hardening of the reactive mass by fast drop of gaseous nitrogen from the reactor encourages the terms of accelerated crystallization of
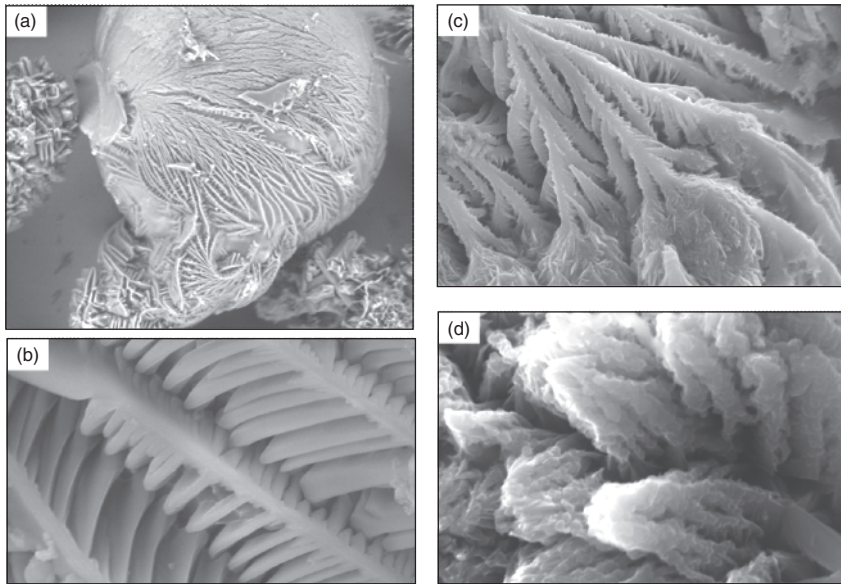
Figure 1.8 Si_3N_4 crystal morphology in the presence of fusing agents: (a) spheres; (b, c) dendrite growth; and (d) imperfect Si_3N_4 crystal.

silicon nitride and obtaining of energetically unstable products. This approach results not only in cooling but also sometimes in overcooling of synthesis products to low temperatures with formation of amorphous products.

The morphological pattern of the products of silicon vapor combustion in gaseous nitrogen at condensation synthesis with "skeleton" crystal formation as well as dendrite growth of silicon nitride crystals in melted metal salts proves the existence of the nonequilibrium mechanism of structure formation in the case of SHS. The mechanism appears to be the basis of the conception of nanodispersed particle formation under the combustion mode [28].

We have discussed the formation of β-Si_3N_4 crystals. However, silicon nitride has another modification – α-Si_3N_4, which exists till 1500 °C.

When silicon nitride is obtained by condensation synthesis, in many experiments α-modification is formed along with β-Si_3N_4. At low nitrogen pressures (≤ 1.0 MPa), up to 50 mass% of α-Si_3N_4 are formed. The morphology of α-Si_3N_4 is remarkable for its variety: cotton-like agglomerates, cobweb-like nanofibers, nanotapes, and "nanoflowers" (Figure 1.9a−e). Probably, at the terms of condensation synthesis, α-silicon nitride is formed by the gas-phase mechanism when gas-transport reactions occur with participation of silicon monoxide, which is practically always present in the reactive mass [41].

Nowadays, there are some variations of α-Si_3N_4 synthesis under the SHS mode. A production technology, which allows obtaining nitride with 97 mass% of α-phase, has been developed [34]. The main parameters influencing the formation of α-Si_3N_4 at combustion of silicon in gaseous nitrogen are the synthesis
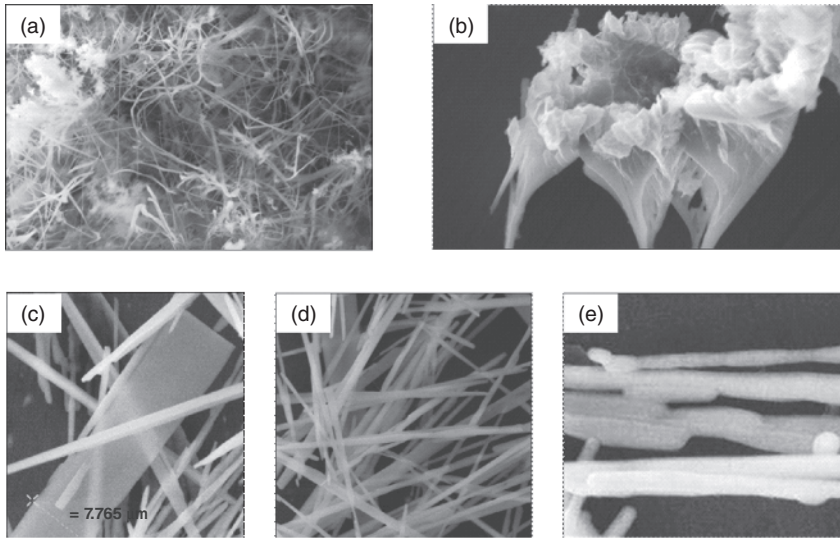
Figure 1.9 Morphology of α- and β-Si_3N_4 nanoparticles obtained at "condensation synthesis": (a) α-Si_3N_4 threads, (b) α-Si_3N_4 "flowers", (c) β-Si_3N_4 tapes, (d) β-Si_3N_4 whiskers, and (e) β-Si_3N_4 tubes.

temperature and presence of gasifying additives decomposing at combustion and providing propagation of gas-transport reactions or formation of intermediate products with silicon, which are precursors in nitride formation. The gasifying additives can be salts (mainly, ammonium halides), organic compounds, polymers, and so on. The morphology of α-Si_3N_4 synthesized with addition of ammonium chlorides and fluorides is presented by two types of silicon nitride particles. At comparatively high contents of halides (up to 15 mass%), thin long crystals – fibers of 100–300 nm in diameter and up to 10 μm in length – are formed, Figure 1.9a. Special studies show that these crystals are formed due to the complicated chemical transformations of ammonium chloride to diimide $Si(NH)_2$ at the reaction with silicon. The diimide is an intermediate compound at nitride synthesis and has a "polymer" structure, which is "memorized" at diimide transformation to nitride. By this time, an SHS technology of filamentary α-Si_3N_4 has been developed with the product output of 100%. At lower temperatures (<1500 °C) and realization of gas-transport reactions with some amount of gasifying additives (<3%), the powders of α-silicon nitride can be synthesized as fine crystals of 60–160 nm in size with l/d being close to 1.

Boron Nitride Nanoparticles of boron nitride powders (α-BN) can be obtained by choosing the proper terms of elemental boron combustion in gaseous or liquid nitrogen or boron anhydride (B_2O_3) combustion by the mode called "SHS with a reduction stage" [43]. In the first case, the agglomerates of BN nanoparticles can be separated by means of chemical dispersion (chemical–thermal method of the

synthesis product treatment). In the second case, the combustion products are treated with acids (leaching) in order to remove the byproduct – a reducing metal oxide. The mechanism of nanodispersed boron nitride formation under the SHS mode appeared to depend greatly on the composition and structure of the reagents participating in the synthesis, particularly on the state of elemental boron, which can be obtained by various methods and, therefore, can have different structures: amorphous, crystal, and so-called polyboride, which contains some amount of magnesium higher borides. The purest pyrolytic boron (in common use – "black boron") is obtained by thermal decomposition of diboranes. The main substance content is 99.7 mass%. Black boron is an ultradispersed powder containing a nanosized component. Its melting point is from 2303 to 2573 K. Nitriding of superpurified powder of extra-pure boron was carried out at $P = 8 - 1000$ MPa [4, 8, 22]. At $P_{N_2} = 150$ MPa, the combustion temperature achieves $2473 - 2523$ K; the powders do not sinter and preserve the porosity which is necessary for nitrogen to access the reaction zone during the entire period of nitriding. Combustion of extra-pure black boron with specific surface area of $12 - 17$ m^2 g^{-1} in extrapure gaseous nitrogen (oxygen content <0.03%) is the simplest method which allows synthesizing boron nitride nanoparticles in *statu nascendi* [44, 45]. Due to the nitriding volume effect, the completeness degree of boron transformation to nitride is 0.99. The investigation on boron nitride morphology and particle size proves that the particles of hexagonal BN have a laminar structure with the plates of <100 nm thick. Besides the laminar particles of boron nitride, those of nonperfect icosahedral structure are observed, Figure 1.10a,b. These results can be connected with the following peculiarities of extra-pure boron nitriding under the combustion mode. Elemental boron is known to begin interacting with nitrogen at ~837 K; at 2273 K, it transforms to nitride with 99.5% output. Below this temperature (2273 K), the initial boron does not sinter at combustion, and dilution of the reactive mass with boron nitride forming at the temperature lower than that of combustion hinders the further sintering of the final product. BN plates are nanosized in two dimensions. Probably, the particles of nonperfect icosahedral structure appear due to the exothermic process of amorphous boron transformation to crystal β-rhombohedral modification at 2253 K [46], which after nitriding makes a certain amount of nitrogen as crystals, while the laminar particles of
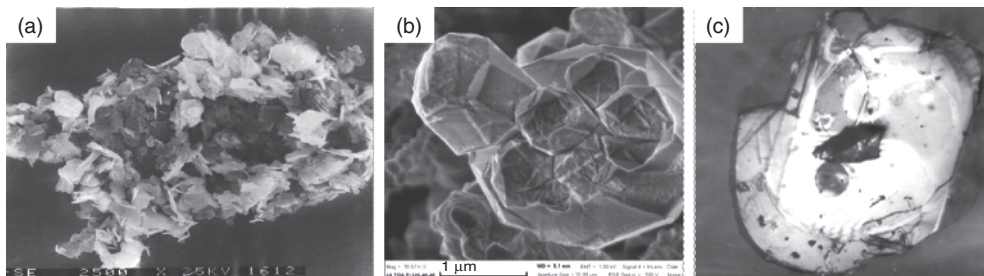
Figure 1.10 Morphology of boron nitride powders: (a) transparent crystals, (b) imperfect icosahedron, and (c) cake of molten BN particles, $d < 50$ nm.

boron nitride are formed only due to the volume effect of the nitriding reaction of ultradispersed boron without agglomeration.

Combustion of black, extra-pure boron powder at high nitrogen pressures (100–150 MPa) and $T > 3000$ K results in appearance of fused transparent particles of <50 nm in size and cakes (ingots) of boron nitride. X-ray analysis of these particles, Figure 1.10c, proves that they appear to be boron nitride single crystals with crystal lattice parameters corresponding to American Society for Testing and Materials (ASTM) ($a = 2.504$ Å; $b = 6.661$ Å). Combustion of elemental boron in liquid nitrogen in specially designed sealed cryogenic SHS reactors by an original method is a unique experiment of boron nitride synthesis [8, 47, 48]. Theoretical calculations show that at liquid nitrogen defrosting in such reactors, nitrogen pressure can achieve 1000–2000 MPa. Such reactions used boron powder, compacted samples, various additives (NH_4Cl, MgB_2), and metal catalysts for synthesizing cubic β-modification of boron nitride (borazon): Li, LiN, MgB_x, Sn, Pb, and so on. For the first time, β-BN (wurtzite-like form) was discovered at X-ray analysis of boron combustion products in the mixture with metal magnesium. In those experiments, α-BN_{hex} was also detected as thin laminar transparent crystals of 0.5 mm in size. It can be compared to borazon by its chemical stability. Formation of this nitride as "ingots" of 6 g in weight was observed along the entire reactor. The product was considered to appear as a result of the back transformation of β-BN → α-BN during the reactive mass cooling. The borazon crystals separated after the reactive mass treatment with $NaOH + Na_2CO_3$ and precipitated in bromform (~1%) were 100–150 μm in size.

But it should be noted that the experiments with boron combustion in liquid nitrogen in sealed reactors were rather dangerous. In some experiments, the pressure leaps higher than 20 kbar resulted in combustion transition to detonation and even the installation destruction as well as acid treatment of the reaction products was followed by shots with flame. Obviously, some by-products or intermediate ones as explosive azides can be formed at fast cooling of the reactive mass.

The mechanism of α-BN formation at combustion of elemental boron or boron with B_2O_3 or halogenides or MgB_x (polyboride), or at SHS with magnesium or boron reduction is different. All these cases demonstrate the possibility of gas-transport reagent formation, which provides the nitriding reaction transition to gas phase. The similar behavior was observed at nitriding of black boron with boric anhydride additives in gaseous nitrogen.

According to thermodynamic calculations, such gaseous products as B_2O_2(g), B_2O_3(vap), BO(g), and B_2O(g) can be formed in such cases at high combustion temperatures. The main compound is B_2O_2. The process of nitride formation with B_2O_2 can occur in the following way:

$$B + B_2O_3 \rightarrow B_2O_2 \tag{1.2}$$

$$B_2O_2 + N_2 \rightarrow BN + O_2. \tag{1.3}$$

Summarily, the reaction can be presented as follows:

$$B + B_2O_3 + N_2 \rightarrow BN + O_2. \tag{1.4}$$

At combustion of magnesium-reduction system of $B_2O_3 - Mg - N_2$, the process occurs within two stages: reduction of B_2O_3 by magnesium and nitriding of the product. It can be presented as follows [43]:

$$B_2O_3 + 3Mg + N_2 \rightarrow 2BN + 3MgO \text{ (a cake BN/MgO).} \qquad (1.5)$$

Gaseous boron oxides are of great importance in the formation of boron nitride. The final product – boron nitride – is separated from the reactive mass by being treated by acids or water, then it is subjected to "chemical dispersion" with pre-set solvents. The primary boron nitride particles, which have not recrystallized at cooling, are preserved and separated; boron nitride is characterized by a high value of specific surface area. In the experiments of $B + B_2O_3$ combustion, BN powder specific surface area was $23 - 27 \, m^2 \, g^{-1}$; in the experiments with magnesium reduction, it grew up to $59 \, m^2 \, g^{-1}$. Boron nitride particles can be observed as thin fibers or stretched plates, Figure 1.5f. Their size corresponds to that of nanoparticles.

But it is rather difficult to use polyboride as an initial source of boron for investigation of boron nitride particle formation and morphology, as this product contains a great number of magnesium borides of various compositions – from MgB_2 to MgB_{12}. Their contents in various lots of polyboride can range from 15 up to 85 mass%. Besides, according to X-ray analyses, this product contains a lot of other impurities: MgO, B_2O_3, B_4C, and so on.

Aluminum Nitride Structure formation mechanism and particle morphology of aluminum nitride powders greatly depend on the combustion terms of aluminum in gaseous nitrogen, particularly on the initial green mixture composition. The problems of aluminum nitride particle formation and size were studied when the pilot SHS technology of AlN production was developed and tested using a large amount of substances in SHS reactors. In these cases, the synthesis parameters were widely ranged, and the combustion products were studied by means of chemical and X-ray analyses and electronic microscopes. When aluminum nitride structure formation mechanism was being studied and optimum synthesis terms were being defined, three variations of SHS were under use: aluminum powder combustion in gaseous nitrogen using aluminum nitride as a diluent; aluminum combustion with halogenides (NH_4Cl, NH_4F, $MgCl$, $AlCl_3$, LiCl, etc.); and aluminum combustion with gasifying additives $NH_4Cl + NH_4F$ (with the green mixture dilution with aluminum nitride). During the experiments nitrogen pressure, initial reactive mass density and weight, particle size of aluminum powder and the diluent (AlN), and the number of additives were changed. Besides the experiments in aluminum combustion in SHS reactors, the combustion mechanism under the terms of the "condensation synthesis" (with aluminum evaporation) and synthesis of nitride at combustion in liquid nitrogen were studied.

At synthesis of aluminum nitride powders in gaseous nitrogen with the green mixture dilution with nitride, the dilution degree influences greatly the aluminum nitride particle size and morphology and defines practically the combustion
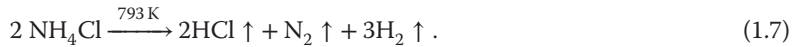
temperature [34, 49]. When the diluent content is 80 mass%, the synthesis temperature is 1843 K. The particle of different shapes are observed: conglomerates of particles of $0.5-1\,\mu m$ size, spherical conglomerates of $1-2\,\mu m$ diameter consisting of separate particles of $0.1-0.5\,\mu m$, and plates or flakes of $\leq 0.2\,\mu m$ thickness. Aluminum nitride powders are characterized by high specific surface area and absence of sintering traces. When the number of the diluent was decreased to 70 mass%, the combustion temperature grew up to 2263 K. Under such terms, aluminum nitride was formed by equiaxial particles of $2-5\,\mu m$ in diameter as conglomerates of $20\,\mu m$ in size. With the further decrease in the amount of the diluent, the growth of separate particles as well as conglomerates of the synthesized nitride was observed. At nitrogen content of 50 mass% in the green mixture ($T_c = 2973$ K), the particle shape and size change drastically. Figure 1.11a shows the fracture surface of AlN cake synthesized from the green mixture consisting of 50 mass% of aluminum and 50 mass% of nitride. The cake contains uniform faceted crystals of $25-30\,\mu m$ in size. These crystals could appear from nitride melt developing at high temperature under nitrogen pressure at the terms of fast heating ($\sim 10^4\,\mathrm{K\,s^{-1}}$). In this case, AlN melting point is higher than the dissociation temperature (2773 K) for the atmospheric pressure but lower than that (3303 K) for the synthesis under nitrogen pressure. A molten AlN sample is shown in Figure 1.11a. It has a form of laminar cakes of $15\,\mu m$ size with "introduced" symmetrical crystal "nests" of ~ 20 nm diameter. The further decrease in the diluent content to 30 mass% made the combustion temperature of aluminum close to the dissociation temperature of nitride. It achieved 3293 K. In the reactive mass, mainly in cavities and hollows of the cake, some foam-like formations appeared with a very fine structure; web-like fibers of $\leq 0.1\,\mu m$ thickness and up to $20\,\mu m$ length; needle-like crystals with the sizes of $1-2$ and $20\,\mu m$, correspondingly. Such particles of aluminum nitride prove the existence of gas-phase mechanism of nitriding stipulated by high synthesis temperatures, which provide aluminum evaporation and make the existence of gas-transport agents, for example, Al_2O, possible. There is one interesting fact – a
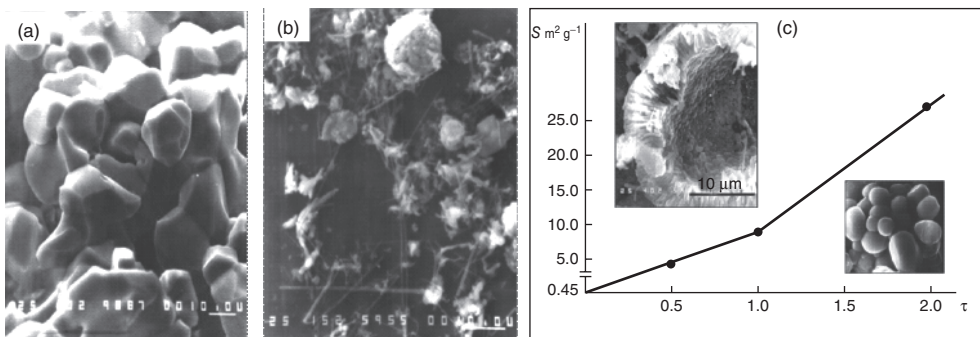
Figure 1.11 Aluminum nitride particle morphology: (a) fracture surface of AlN cake, (b) general view at $T_c = 1890\,°C$, and (c) conglomerate disintegration by "chemical dispergation."

change in AlN color shade (from light-gray to yellow) depending on the synthesis terms. The shade is determined by the particle size and shape. The particles of $0.2-1.0\,\mu m$ size have a light-gray shade; white or yellow color is characteristic of the spherical particles of $2-15\,\mu m$. Flat particles provide light-blue color, and faceted crystals are light green.

As it was mentioned above, the application of gasifying agents was suggested to decrease the combustion temperature and velocity and loosen the reactive mass. AlN synthesis with participation of NH_4Cl is followed by a decrease in the combustion temperature as some part of the reaction heat is spent on NH_4Cl transformations (sublimation and decomposition):

$$NH_4Cl \xrightarrow{611\,K} NH_4Cl \uparrow \tag{1.6}$$

$$2\,NH_4Cl \xrightarrow{793\,K} 2HCl \uparrow + N_2 \uparrow + 3H_2 \uparrow. \tag{1.7}$$

The maximum decrease in the combustion temperature is observed at NH_4Cl content of 10 mass%. The sharp drop of the temperature is connected with the effect of gases forming at NH_4Cl decomposition. Ammonium chloride sublimation and decomposition occur at $\sim\!800\,K$ in the zone of the green mixture warming. So, HCl and H_2O accumulate before the combustion front and decrease nitrogen concentration before the reaction zone. It becomes more apparent at low nitrogen pressure.

Ammonium chloride, which is contained in the green mixture, also affects aluminum nitride particle morphology. The influence of ammonium chloride on AlN particle shape and size is well seen at high content of NH_4Cl (10 mass%) and minimum combustion temperature, that is, at combustion under the conditions close to threshold [34]. In Figure 1.11b, we can see the general view of aluminum nitride powder obtained at $P = 4\,MPa$ and $T_c = 1890\,K$. It is obvious that thread-like crystals exist along with spherical particles. It supports the idea that
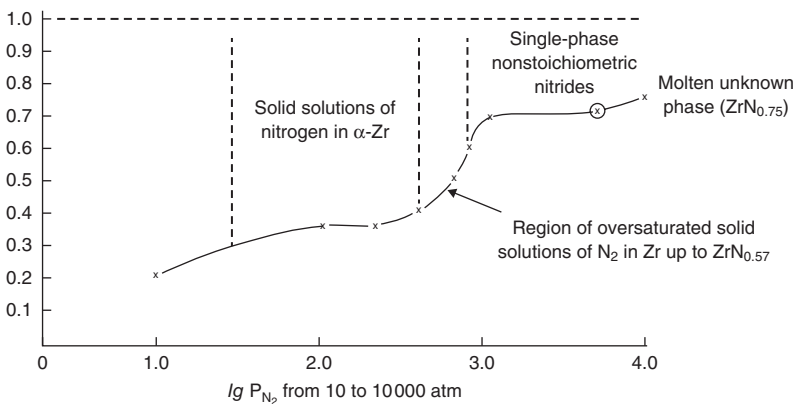
Figure 1.12 Dependence of zirconium combustion product composition on nitrogen pressure.

the structure formation mechanism changes to the gas-phase mechanism in which gas-transport agents (the products of ammonium chloride decomposition and intermediate products, e.g., $AlCl_3$) play an important role. Besides, the dispersion degree of aluminum initial powders is rather significant for formation of ammonium nitride granulometric composition and AlN particle morphology [50]. In the case of polydispersed aluminum particles, the nitriding reaction has two stages. At first, fine aluminum particles ($d < 5\,\mu m$) react with nitrogen in the combustion front; the combustion temperature attaining $1800 – 1900\,K$ (at ~15 mass% of fine particles). It provides the sufficient thermal conditions for nitriding of coarser aluminum particles on the stage of after-burning. At higher pressures ($>5.0\,MPa$), nitriding almost finishes within the combustion stage. When AlN is synthesized at the combustion threshold ($\leq 4.0\,MPa$), fine aluminum particles form thread-like crystals and coarse ones produce spherical formations consisting of submicron particles. We can conclude that the following terms ensure the formation of nanosized thread-like AlN crystals: fine initial powders of aluminum, low pressures of gaseous nitrogen ($\leq 4.0\,MPa$), low combustion rate elongating the isothermic combustion terms, and stable thermal regime of after-burning, which provides the growth of thread-like crystals. Equiaxial submicron particles can be obtained at "disintegration" of coarse spherical formations. Only in this case it is possible to determine the real specific surface of the synthesized AlN powder [4]. The optimum way of submicron AlN powder separation from the spherical conglomerate coat is "chemical dispergation" destroying the interlayers between the grains, Figure 1.11c, or use of the jet-mill of the type AFG-100 of "Alpine" Company (Germany); its operation being based on substance milling in the air counterflows.

Ammonium fluoride also decomposes at combustion:

$$NH_4F \xrightarrow{425\,K} NH_3 \uparrow + HF \uparrow \tag{1.8}$$

$$2NH_3 \xrightarrow{793\,K} N_2 \uparrow + 3H_2 \uparrow. \tag{1.9}$$

Aluminum nitriding with ammonium fluoride is more intensive in comparison with that with ammonium chloride. It can be explained by chemical activity of hydrogen fluoride. It dissolves the alumina film, which always exists on aluminum particles and accelerates the reactive ability of the green mixture. When AlN is synthesized in the presence of NH_4F, spherical AlN particles are mainly formed [34]. Obviously, it occurs due to the formation of a liquid film of AlF_3 on the surface of a liquid aluminum drop during the nitriding processes by the vapor–crystal mechanism. The quantity of the evaporated aluminum depends on the thickness of AlF_3 film on the liquid aluminum drop. The portion of the evaporated aluminum "bubbles" through the film and is nitride, forming a hollow spherical conglomerate AlN. Its particle size depends on the combustion temperature and ammonium fluoride quantity in the green mixture, that is, on the quantity of AlF_3.

So-called condensation synthesis was carried out. It included evaporation of aluminum in nitrogen atmosphere without gasifying agents. Nitrogen pressure was ranged from 1.0 to 4.0 MPa. Aluminum is known to have rather low melting

point (931 K), so at burning of pure aluminum, nitride formation involves several stages: Al melting, Al vapor diffusion in nitrogen, reaction of Al vapors with nitrogen, and formation of nitride particles. AlN is formed as spherical particles with the shell of aluminum nitride. The evaporated aluminum portion, which is inside the sphere, "bubbles" through the surface nitride film and is subjected to nitriding in the intergranular space forming flexible laminar rods of AlN. The size of some aluminum nitride laminas is <50 nm.

Therefore, we can synthesize aluminum nitride powders in a wide range of sizes – from nanosized to micron powders with various morphologies (spherical, laminar, thread- and needle-like) by changing aluminum combustion temperature, nitrogen pressure, and the initial mixture composition. Each size can be considered as optimum for specific applications.

1.3

Dependence of SHS Nitride Composition and Structure on Infiltration Combustion Mode

The main difference of solid−gas systems from solid−solid ones is the following: the initial reagents are in different states of aggregation and one of them is characterized by high volatility; the amount of the reactive gas (nitrogen) in the pores of the solid sample is not sufficient for spontaneous propagation of the combustion front and formation of the final product. The gas is brought to the reaction zone during combustion. It is done in a hydrodynamic way by means of filtration along the porous sample. The filtration occurs because of the pressure difference at the combustion front and in the sample volume due to nitrogen absorption in the combustion front. So, the combustion front acts as a pump sucking the gas in pores from the environment. If the sample remains porous after the combustion front propagation, the gas can be supplied to the reaction zone along the unburnt and burnt-up parts of the sample simultaneously. This conclusion of the first investigations of SHS combustion in solid−gas systems [1, 8, 51] appeared to be the fundamental conception for the development of a separate direction of SHS called "infiltration combustion" [52]. The peculiarity of the supply of one of the reagents to the reaction zone has facilitated realization of various experiments and obtaining of valuable results for both combustion theory and application. Among the results is a discovery of "spin" combustion, various modes of the combustion front propagation (stationary, layer-by-layer, surface, nonstationary, auto-oscillating, after-burning of the samples warmed-up by the combustion front, combustion with the product dissociation, etc.) [2, 53−55]. All these concepts have become ordinary for SHS researchers and scientists.

Nitride composition and structure are greatly dependent on the combustion mode or the existence of a phenomenon accompanying infiltration combustion. That is, why it is necessary to work out specific approaches for developing optimum terms of final item production in each system. Nowadays, a lot of experimental studies and theoretical works allow the scientists to foresee the

formation of final products and develop the required terms. These approaches include a decrease in combustion temperature by dilution of initial solid reagents with inert additives or introduction of active additives, dilution of nitrogen with inert or reactive gas, and so on. It is rather easy to predict the influence of such parameters as nitrogen pressure, initial density, size, and shape of burning samples on the final product composition. These parameters are essential in investigation and description of the synthesis process of each system. But spin and auto-oscillating combustion, nitride dissociation, melting of intermediate and final products, evaporation of initial reagents, their results, and influence on the product composition and structure are less described in literature. However, there are many examples, which allow generalizing some specific dependencies of nitride structure and composition on the modes of infiltration combustion.

1.3.1
Two Stages of SHS Process

One of the important results of investigation of infiltration combustion mechanism is the discovery of two stages of the process: burning – after-burning (volume nitriding of the sample heated by the combustion front). It can be demonstrated using the well-known examples of nitriding during SHS of low-melting zirconium and refractory tantalum [4, 9]. Compacted zirconium powders burn at $P_{N_2} > 30$ MPa in the mode of surface combustion with the sample melting without the after-burning stage. In this case, α-solid solutions of nitrogen in metal, oversaturated solid solutions and nonstoichiometric nitrides are formed even at very high nitrogen pressures, Figure 1.12 [8, 47].

Combustion of Ta – N was studied at a wide range of nitrogen pressure (from 2.0 to 300 MPa) [15, 16, 56]. In some cases, tantalum powder was pressed in quartz tubes or cups. Tantalum combustion in nitrogen is carried out in a layer-by-layer mode. Upon studying volume after nitriding (after-burning), a couple of intriguing facts directly concerned with chemical transformations in the combustion front and behind it were revealed. One of these facts is the appearance of the second combustion front when tantalum powder is burnt in quartz tubes, which are sealed at the top end to eliminate gas supply through the combustion products. When nitrogen was supplied only through the initial tantalum powder toward the combustion front, there appeared weakly luminous first combustion front, which was moving fast toward the end of the sample. Arriving at the lower end of the sample, the front produced a flash, then the second combustion front arose; it was brighter than the first one and moved in the opposite direction with deceleration to a complete stop. X-ray analysis of the quenched combustion products showed that during the first front propagation, a solid solution of nitrogen in tantalum and γ-Ta_2N were formed. In the layer where the second front stopped, the combustion product had three phases: in addition to solid solution and γ-Ta_2N, there existed ε-TaN_{hex}. In the layers where the second front propagated in a steady-state mode, the combustion front consisted of a single phase: ε-TaN_{hex}.
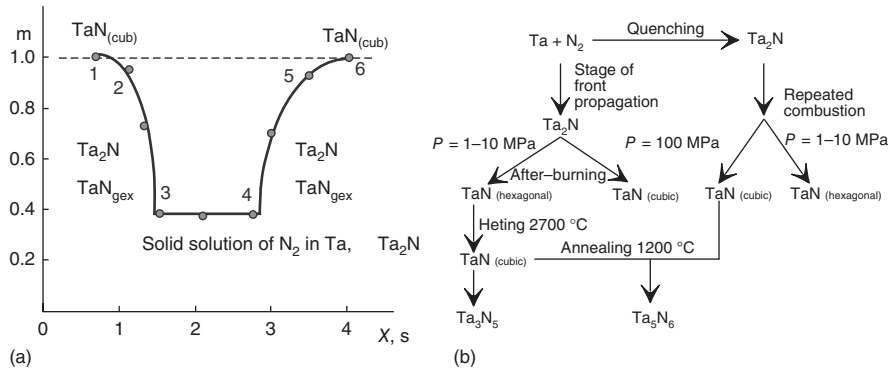
Figure 1.13 Mechanism of tantalum nitride formation: (a) nitrogen concentration along TaN sample and (b) phase formation stages in T−N system.

Two combustion fronts in Ta−N system were observed in the experiments with tantalum powders pressed into quartz tubes (both ends were open to let the gas in). However, in this case, the second front arose, the same as the first one, at the ignition spot and was proceeding in the same direction but with a time delay. Figure 1.13a demonstrates the nitrogen concentration profile along the sample (relative units of m; at $m = 1$, the composition corresponds to the stoichiometric mononitride TaN). The phase composition of the combustion products is given as well. It can be seen that the complete conversion occurs at the ends of the burnt-up sample, whereas in the middle of the sample, only solid solution of nitrogen in tantalum and γ-Ta_2N are formed. The analysis of numerous results obtained during the study of the combustion process in $Ta + N_2$ system revealed the multi-step character of the interaction between tantalum and nitrogen and determined optimum conditions for synthesizing any phase involved in the SHS mode. The results of the experiments in synthesizing different phases in Ta−N system are shown in Figure 1.13b. The experiments prove that in the preheating zone adjacent to the combustion front, nitrogen is practically always dissolved in tantalum, forming solid solution. This stage is exothermic, but as the heat release is not enough, the reaction zone propagation in the form of the combustion front is not self-sustained. The combustion front propagation is governed by thermal flows of strongly exothermic reaction of γ-Ta_2N. In the after-burning wave, the third exothermic stage occurs – ε-TaN_{hex} is formed according to the following equation:

$$Ta_2N + \tfrac{1}{2} N_2 = 2TaN + Q \text{ (J)}. \tag{1.10}$$

In the after-burning zone, the fourth stage takes place – it is endothermic transition of ε-TaN_{hex} to δ-TaN_{cub}. δ-TaN_{cub} is thermodynamically stable only at high temperatures and can be retained after combustion due to very rapid cooling, in fact in a quenching mode.

It should be noted that δ-TaN_{cub} has never been produced by conventional methods. We were the first who synthesized it by tantalum combustion in liquid nitrogen [56]. Its structure was investigated by Shekhtman using X-ray

analysis. Later, Petrunin with coworkers [57] studied δ-TaN$_{cub}$ more thoroughly using neutron diffraction method. The compositions with "superstoichiometric" nitrogen content (TaN$_{1.2}$) were given the priority in this study. Nitrogen atoms were shown to be located in octahedric interstitial sites; metal sublattice having defects. Consequently, more correct chemical formula of this nitride is δ-Ta$_y$N ($y < 1$), it is different from the commonly used one in literature – TaN$_x$ ($x > 1$). It should be mentioned that because of this particularity of its structure, δ-TaN$_{cub}$ differs from other nitrides of transition metals of the IV–VI of the periodic table, which have cubic lattice of NaCl type. The vacancies in the crystal lattice are probably the cause of anomalously high values of microhardness of δ-TaN$_{cub}$ (3200 kg mm^{-2}) in comparison with that of other nitrides, which never exceed 2000 kg mm^{-2}.

During the experiments proving the existence of two stages of the nitriding process, we observed some changes in sample weights during the reaction. A special fast automatic balance was designed for this purpose [8]. The balance meets the requirements of the investigation and has the following operation characteristics:

- characteristic time – 0.03 s max;
- resolution ability – 0.05 g;
- maximum sample weight – 10 g; and
- a range of sample weight variation – 0–500 and 0–1000 mg.

The balance is a unique device considering all the peculiarities of fast high-temperature combustion processes including convection flows, changes of buoyancy force with pressure, and so on. Figure 1.14a,b demonstrates a typical curve of the weight gain of a zirconium sample during combustion at nitrogen pressure of 10 MPa [8, 28, 47, 51]. The weight gain consists of two stages: a fast stage ($\sim$1 s) and a slow rather long stage of enrichment. The first stage corresponds to the front

(a) (b)
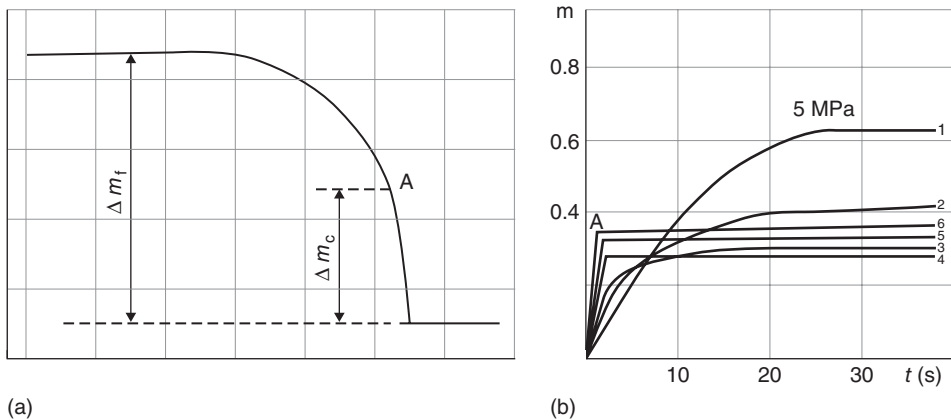
Figure 1.14 Gravimetric curves of zirconium nitriding: (a) sample weight gain at nitriding (Δm_c – combustion stage, Δm_f – total gain) and (b) gravimetric curves of nitriding at various nitrogen pressures (5, 10, 30, 50, 70, 100 MPa); point A corresponds to the end of combustion.

motion along the sample; point A corresponding to the moment when the front achieves the lowest of the sample. It was called the stage of the combustion front propagation; the weight gain is Δm_c. The second stage corresponds to the volume after nitriding; it is the stage of after-burning. The total weight gain after two stages is Δm_f. But we must remember that it is not always possible to separate two stages of the combustion process of porous samples in gaseous nitrogen. In the case of slow burning metals, the process of after-burning can make a substantial contribution to Δm_c during the period when the combustion front has not achieved the sample end. It is well observed in niobium combustion. In the case of fast burning metals, after-burning might affect Δm_c when the samples under use are long. However, the chance is minimal.

One of the most interesting systems to be used for investigation of burning–after-burning processes and final product formation is that of hafnium–nitrogen characterized by the highest calculated adiabatic combustion temperature ($T_{ad} = 5100$ K) and rather low melting point ($T_m = 2495$ K). Due to its high reactivity with nitrogen and existence of a single nitride with a homogeneity range of $HfN_{0.74}$–$HfN_{1.13}$ and a single solid solution with a homogeneity range of up to $HfN_{0.41}$, the system of Hf–N can burn at various modes: stationary, spin, self-oscillating, with appearance of the second combustion front (Figure 1.15) [58]. The stationary front propagation is observed at $P_{N_2} > 1.0$ MPa. At $P < 1.0$ MPa (up to 0.1 MPa), the combustion front consists of bright points moving in different directions, and at $P_{N_2} \sim 0.1$ MPa and lower, typical spin combustion is observed. At relatively high sample densities ($\Delta > 0.6$), self-oscillating combustion takes place. Appearance of the second combustion front at $P_{N_2} > 1.0$ MPa is of great interest. It follows the main front as a bright and wide glow downwards with the same velocity. The sample quenching in argon immediately after the first front propagation shows that at any pressures nitrogen content in the sample
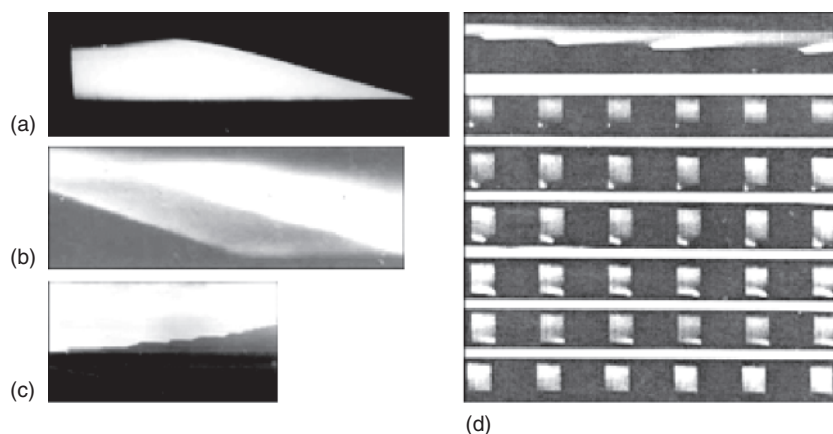
Figure 1.15 Photographic record of hafnium combustion in nitrogen at $P_{N_2} = 6.0$ MPa: (a) stationary combustion, (b) second front, (c) self-oscillating combustion, and (d) record of spin combustion at $P_{N_2} = 6.0$ MPa and $P_{Ar} = 0.1$ MPa.

center is very low (<1 mass%). On the sample surface at any P_{N_2}, only hafnium nitride is detected as a thin loose layer. After the second front propagation, the entire sample is hafnium mononitride. Therefore, the primary combustion process in the system of Hf−N occurs under the surface mode and retains permeability sufficient for propagation of after-burning. The appearance of the second front is explained by the combination of two factors: heating of the sample internal layer by the first combustion front without nitriding and retaining of the permeability, which promotes layer-by-layer after-nitriding of the sample. Figure 1.16 demonstrates gravimetric curves of porous hafnium nitriding in comparison with zirconium at P_{N_2} = 2.0 MPa when zirconium is completely melted and becomes impenetrable for nitrogen. Point A corresponds to the moment when the first front in the experiments with Hf and the combustion front in those with Zr reached the bottom end of the sample. In the case of Zr, nitriding is over, only solid solution of nitrogen in zirconium is formed. In the case of Hf, the result is different. Before point A, hafnium nitride is formed in a thin surface layer, the second front (point B) contributes greatly to the nitriding degree (up to $HfN_{0.56}$). The existence of the surface combustion at the retained sample permeability is connected with the well-known high hafnium reactivity in the reactions with nitrogen. Any quantity of nitrogen on the sample surface reacts with the metal and forms nitride. Only the layer thickness is different. The after-burning stage – volume after nitriding of the samples heated by the combustion front – plays an important role in the final product formation. The discovery of the after-burning stage appeared to be critical for comprehension of metal hydrogenization at the SHS mode and determination of optimum terms for obtaining a wide range of metal hydrides and alloys by combustion. These compounds are known to be thermodynamically unstable.

The after-burning stage is not only an interesting phenomenon of incomplete reaction in the combustion front but also plays a specific role in obtaining high-quality final products. Nowadays, this stage is widely used in the development of novel technologies and production of nitrides by the SHS method, which is not surprising. According to Merzhanov [28], the after-burning stage is directly connected with such processes as substance postfrontal transformations. They
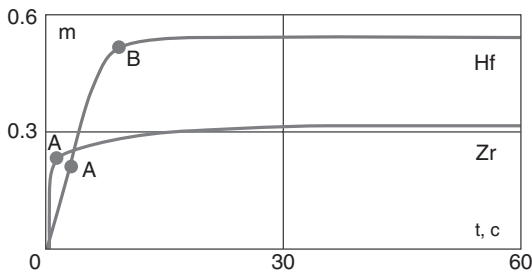
Figure 1.16 Gravimetric curves of hafnium and zirconium nitriding at P_{N_2} = 2.0 MPa, A – sample end and B – Hf second front.

occur far behind the combustion front and do not affect its propagation. Phase and structural transformations are of important role too. They define the final product composition, structure, and properties. At present, there are a lot of papers dedicated to the structure formation mechanism [59–61]. Many of them formed the foundation of a new scientific direction, which was called "structural macrokinetics" (study of direct and back links between chemical reaction processes, heat and mass transfer, phase and structure transformations).
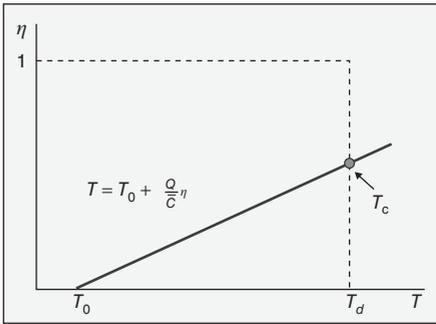
1.3.1.1 Nitride Dissociation

Another important thing in the synthesis of final products by combustion of metals and nonmetals in nitrogen is the possibility of dissociation of the obtained compounds. The paper [8] was the first to define a change in Gibbs function ΔG of the system Me–N when determining the direction of the reaction:

$$\text{Me}_s(l) + \text{ }^1\!/_2\,\text{N}_2 \rightleftharpoons \text{MeN}_s(l) \tag{1.11}$$
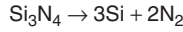
at the combustion temperature, and calculating the equilibrium constants and nitrogen pressure. The positive values of ΔG and low equilibrium constants prove that in all the systems under study (Al–N, B–N, Zr–N, Ti–N, Hf–N, V–N, Nb–N, Ta–N), at the combustion temperature, the reaction shifts left, that is, nitride dissociation is possible. Due to the calculated nitrogen pressures, the strongest dissociation is expected in the case of combustion of aluminum, then that of boron, and at last of transition metals – titanium and zirconium. Thermodynamic analysis of combustion temperature and product composition was carried out at the constant pressure for two systems: aluminum–nitrogen and boron–nitrogen at various ratios of the initial components (from stoichiometric to a remarkable excess of nitrogen) and at two values of nitrogen pressure: 0.1 and 10 MPa. The calculations showed that the absence of aluminum nitride dissociation at 0.1 MPa was observed only at a large excess of nitrogen ($\gg 3$ mol instead of 0.5 mol by the reaction $\text{Al} + 0.5\,\text{N}_2 = \text{AlN}$). Besides, the combustion temperature decreased to 1818 K, that is, the combustion process was critical and could fail. Dissociation of all the nitrides under study can be suppressed completely with an increase in pressure and depending on the initial element properties. Later, the obtained results were proved in the experiments and technological works. They gave start to the development of the method of dissociation suppression of the combustion products by a significant decrease of the combustion temperature by diluting the initial solids with various additives. The thermal effects of nitride formation are so high that it is possible to decrease the temperature in a wide range without fear of the process being stopped. The model of high-temperature dissociation was described in [62]. The simplest example of the product dissociation in the combustion wave $\text{AB} \rightarrow \text{A} + \text{B}$ (complete dissociation to the elements at a preset dissociation temperature) was described by Merzhanov, Figure 1.17, using the reaction

$$\text{Si}_3\text{N}_4 \rightarrow 3\text{Si} + 2\text{N}_2. \tag{1.12}$$

$$T = T_0 + \frac{Q}{c}\eta$$

Example

$$Si_3N_4 \rightarrow 3Si + 2N_2$$

Figure 1.17 Product dissociation in combustion wave: (the simplest case: $AB \rightarrow A + B$); T_0 – initial temperature, T_d – dissociation temperature, T_c – combustion temperature, η – degree of nitriding completeness, and c – thermal capacity.

The role of dissociation in silicon nitride production was thoroughly studied in [32]. Within the experiments, we can see that the temperature of silicon combustion in nitrogen does not depend on the degree of the initial mixture dilution with silicon nitride and grows monotonously from 2200 K at $P_{N_2} = 6$ MPa up to 2400 K at $P_{N_2} = 50$ MPa, Figure 1.18a. The combustion velocity increases with the pressure growth. At $P_0 = 12$ MPa, the combustion temperature is 2250 ± 50 K and it does not depend on dilution (α). We could not achieve steady-state combustion in region 1 at $\alpha \leq 0.1$. The system does not burn either if the dilution with nitrogen is higher than 70% ($\alpha \geq 0.7$; region III). These peculiarities of silicon combustion in nitrogen encouraged us to study thoroughly the system combustion regularities connected with gas penetration in the combustion zone and influence of silicon melting and silicon nitride dissociation. According to literature, silicon nitride


(a)

(b)
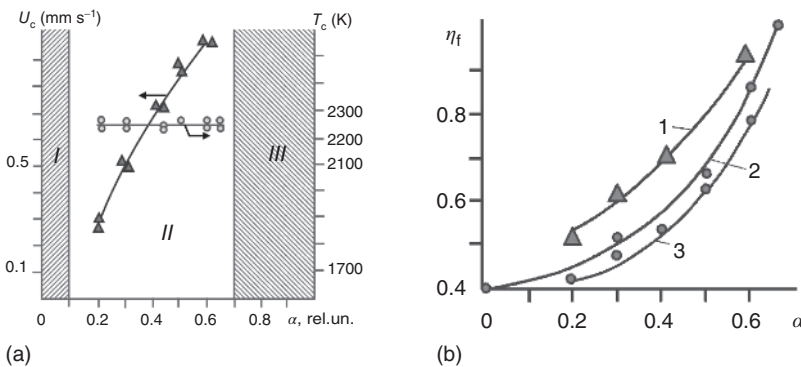
Figure 1.18 Silicon infiltration combustion in nitrogen: (a) dependence of silicon combustion velocity and temperature on dilution (α) with α-Si_3N_4 and (b) dependence of nitriding completeness degree (η) on dilution (α): 1 – natural cooling, 2 – theoretical calculation, and 3 – quenching.

decomposes to liquid silicon and gaseous nitrogen. When comparing experimental and equilibrium values of T_c and η_f (conversion) degree, we can conclude that silicon combustion in nitrogen is a thermodynamically equilibrium process and can be described using the model of high-temperature dissociation. It is proved by the dependence of η_f on α (Figure 1.18b). η_f is obvious to grow with α. The excess of η_f for the samples, which were cooled without quenching in comparison with that obtained by theoretical calculations, is explained by existence of the after-burning zone characteristic for this system.

The value of the combustion temperature with due regard to dissociation of the final product must be determined especially for the development synthesis methods and production technologies of high-quality nitrides with preset particle shape and size. Let us recall our work in the synthesis of aluminum nitride by combustion of aluminum mixtures with aluminum nitride at various dilution degrees and combustion parameters [34]. Our investigation proved that the temperature decreased with a decrease in nitrogen pressure, Figure 1.19a. The minimum combustion temperature of the green mixture with aluminum content of 18 mass% is 1743 K. The obtained aluminum nitride appears to be a cake homogeneous along the entire volume of the sample. When aluminum content was increased to 50 mass%, 10–15% shrinkage of the sample was observed in comparison with the volume of the initial mixture; and the temperature grew up to 2973 K. The further increase in aluminum content to 70 mass% made the temperature of combustion close to that of nitride dissociation (∼3293 K). Aluminum nitride dissociation temperature at 7 MPa is 3303 K. The nitride obtained in this case is a porous cake. Figure 1.19b shows dynamics of the temperature variation in the combustion front for the compositions with 70 and 50 mass% of Al. The heat pattern has two peaks. In this case, AlN synthesis is characterized by fast nitrogen absorption from the

(a)

(b)
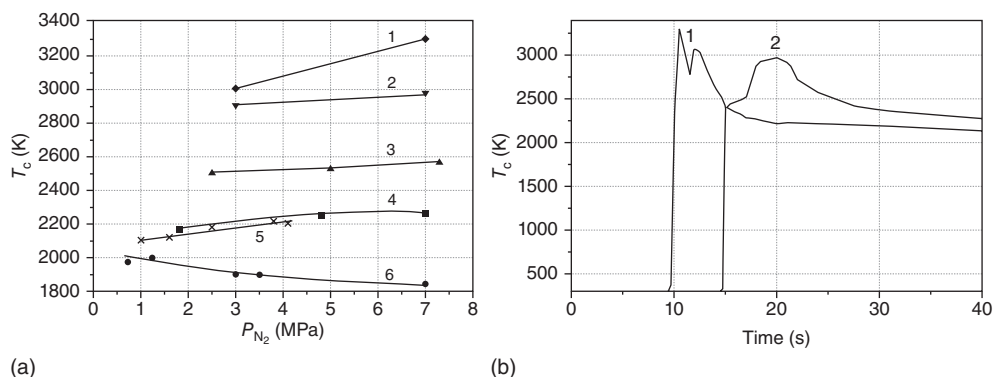
Figure 1.19 (a) Influence of initial pressure on combustion temperature of green mixtures of various compositions (1 – 70% Al, 2 – 50% Al, 3 – 40% Al, 4 – 30% Al, 5 – 25% Al, and 6 – 20% Al) and (b) temperature profiles of the combustion front at P_{N_2} = 7 MPa, 1 – 70% Al, 2 – 50% Al.

reactor volume due to high combustion velocity and high Al content. In the combustion wave, T comes closer to the dissociation temperature but does not exceed it. The effect of high temperatures of Al combustion close to that of dissociation on AlN particle size and morphology was considered in part 2 of this chapter. It should be only underlined that AlN synthesis at $T > 2973\,K$ results in formation of faceted AlN particles. But as the combustion temperature is close to AlN dissociation point, AlN is also formed from the gas phase and the condensed particles take the form of needle-like crystals.

As it was mentioned in part 2, boron nitride can be obtained as melted particles and laminar single crystals. The main problems at melted boron nitride formation are those of the temperatures of boron nitride melting and dissociation. It is known that the melting point of boron nitride at nitrogen pressure is ~3000 °C, and the temperature gradually grows up to 3500 °C at the pressure of about 8000 MPa. At a further increase, boron nitride dissociates to amorphous boron and nitrogen. Obviously, melting occurs simultaneously with the nitriding reaction, and the melting velocity is controlled by that of the chemical reaction. The temperature is constant and equal to the melting point (T_m). Probably, the chemical reaction takes place before the formation of the composition which can exist as a melt at these terms (P_{N_2} and T_c), that is, to the composition of BN_x, where $x = f\ (P_{N_2}$ and T_c). The melt consisting of liquid boron with nitrogen diluted in it in the amount "admitted" by the external pressure and combustion temperature forms the melting surface. The melt is homogeneous in its composition. During the melt cooling, some transformations can occur: quenching of nonstoichiometric composition as an amorphous compound must have taken place in work [8] when $BN_{0.75}$ was obtained, crystallization by the scheme $(BN_x)(l) \rightarrow BN(s) + B(l)$, when $x < 1$, occurs in most cases, or crystallization by the scheme $(BN)(l) \rightarrow (BN_x)(s)$, if $x = 1$.

Considering the results of these experiments, we can assume that boron combustion at high nitrogen pressures corresponds to the elemental combustion model of the second type, namely, the model of high-temperature melting.

The experiments with other elements (metals) prove that at temperatures higher than the melting point of the solid reagent but lower than the nitride dissociation temperature and at high gaseous nitrogen pressures, nitriding can occur by the liquid-phase mechanism with formation of the solid reagent melt, development of saturated nitrogen solution in liquid nonmetal or metal with the composition "admitted" by the external nitrogen pressure and the combustion temperature of the composition, and the following cooling with the yield of melted nitride crystals.

The weakest point in the discussion on the combustion model of high-temperature melting is the absence of the data of nitrogen dilution in boron, silicon, and metals in a liquid state, that is, the absence of equilibrium phase diagrams at $P = 0.1\,MPa$ as well as at $P > 0.1\,MPa$. But if the combustion model is true, it is possible to plot the liquidus line for Al−N, B−N, and Si−N by plotting the dependence with the quenched products: $T_{com} = f\ (m_{quen})$, where (m_{quen}) is the composition due to which T_c develops in the combustion front and $T_c = f\ (P_{N_2})$.

1.3.1.2 Role of Nitrogen Admission to the Reaction Zone

The infiltration mechanism of gaseous nitrogen admission to the reaction zone is very important for organization of the entire process and combustion product formation. Nitrogen admission to the reaction zone is another significant factor for attaining nitriding completeness and development of the terms providing formation of nitride particle phases and structures. From the viewpoint of gaseous reagent supply, we should remember that there can be some diffusion difficulties of nitrogen admission to the reaction zone. In this case, the real combustion temperature can be much lower than its thermodynamic equivalent and the combustion process can result in incomplete substance transformation to nitride. From the viewpoint of solid reagent behavior at combustion, we can expect its melting or melting and decomposition of the intermediate products, insufficient initial permeability of the samples under study, low values of nitrogen pressure, and so on. They can lead to infiltration difficulties for gaseous nitrogen to admit. The diffusion mode of gas supply to the combustion front can be established by dilution of nitrogen with other gas, for example, argon [8, 12], which can gather close to the reaction zone. Figure 1.20a shows the dependence of zirconium combustion velocity on the amount of argon in the mixture of nitrogen−argon at constant nitrogen pressure. Transformation of infiltration combustion to the diffusion mode results in a sharp slowdown of the combustion process. Even small additions of argon decrease zirconium combustion velocity ∼5 times, and addition of ∼0.26 parts results in its complete damping. The results obtained at filtration combustion transformation to the diffusion mode at nitrogen dilution with argon were very important for further development of the new direction in combustion theory and practice, the so-called "spin" combustion, which had not been known before [2, 12, 63]. Since its discovery, the nature and varieties of spin combustion have been of great interest for scientists. But as to the influence of spin combustion on product composition, this direction has not been studied thoroughly. In general, the degree
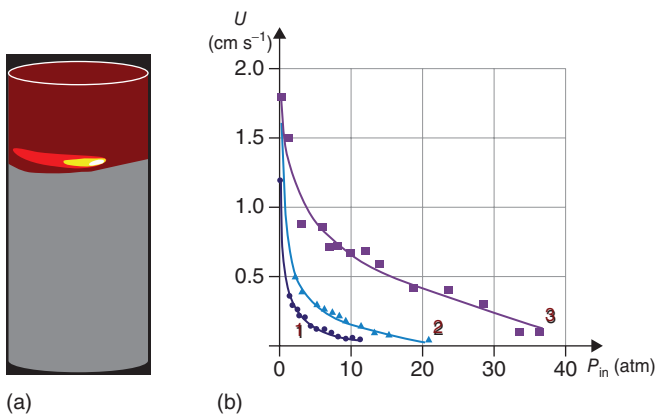

Figure 1.20 Spin combustion: (a) of zirconium and (b) dependence of Zr combustion velocity on argon content in nitrogen at spin combustion.

of the initial solid conversion to nitride depends on the character of spin travel, that is, the hot spot where the reaction is localized and which moves in tangential and longitudinal directions round the sample spirally, Figure 1.20b. The spin wave can move either on the sample surface, and its middle part remains unreacted, or in the whole volume. These phenomena were studied experimentally in [12]. Paper [58] describes the replacement of combustion modes from stationary to spin at hafnium combustion at nitrogen pressure ranging from 2.0 to <1.0 MPa. The combustion product composition at 2.0 MPa corresponded to nonstoichiometric hafnium nitride $HfN_{0.56}$ in the whole volume of the sample, and in the case of spin combustion, the nitride layer was only $1-2$ mm thick, the other part of the sample consisted of pure hafnium.

Not only can an inert gas be used for nitrogen dilution for infiltration combustion transfer to the diffusion type. For instance, in the case of zirconium combustion in the mixture of nitrogen–ammonia or pure ammonia, the combustion velocity drops [8], though ammonia is an active nitriding agent. The slowdown of the combustion front and zirconium nitriding is connected with hydrogen releasing at ammonia dissociation and impeding nitrogen admission to the reaction zone. The similar action is observed in the case of solid additives, which decompose at combustion, for example, halogenides NH_4Cl, NH_4F [34]. Due to accumulation of the gaseous products of their decomposition (H_2, HCl, Hf), a replacement of layer-by-layer combustion by the surface type can be observed.

As it was mentioned above, not only gaseous reagents can make infiltration difficulties at combustion synthesis of nitrides, they can be connected with solids as well. In modern literature, there are a lot of publications dealing with the reasons of various infiltration difficulties and their influence on the nitriding process at combustion: melting of initial reagents, their particle size, lack of nitrogen, high density and dimensions of samples, combustion product dissociation, and so on. They are specific for each system and must be taken into account at search of synthesis optimum terms. Let us consider an example. When optimum terms of aluminum nitride synthesis were being determined [34, 64], the main attention was paid to three technological parameters: nitrogen pressure, initial mixture porosity, and aluminum content in the green mixture. The experiments showed that with an increase in relative density of the initial mixture at $P_{N_2} = 7.0$ MPa, the combustion temperature drops, Figure 1.21a. It is especially noticeable at aluminum content of $50-70$ mass% (AlN is the balance). As AlN is synthesized at rather low pressure, the amount of nitrogen in the pores is not enough for the combustion completeness; the gas must admit to the reaction zone from the reactor through the green mixture layer. An increase in relative density of the green mixture results in nitrogen lack at the combustion front and sharp drop of the combustion temperature and velocity. At the green mixture relative density of $27-32$%, the curves of the combustion velocity (Figure 1.21b) have a horizontal inclined character. It proves the kinetic combustion mode [8]. When the relative density of the green mixture is increased to 40%, the combustion velocity becomes twice lower due to infiltration difficulties. This example illustrates the transfer of the combustion mode from the kinetic type to the infiltration one. The change of the combustion mode led to

(a)   (b)
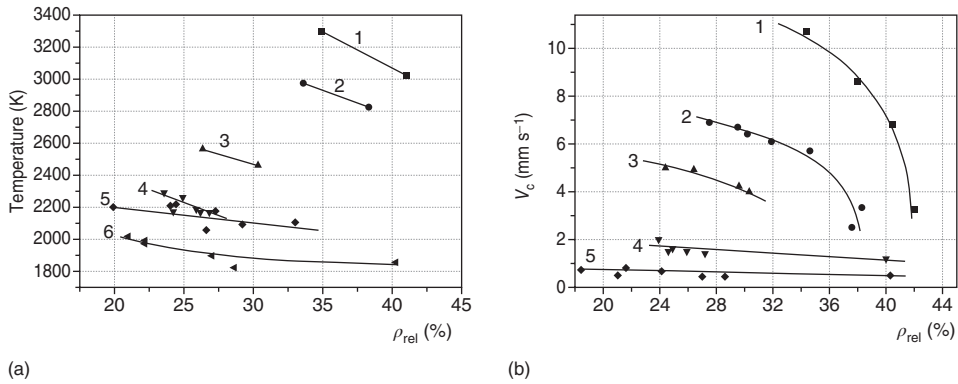
Figure 1.21 Al–N combustion temperature dependence on relative density of the green mixture: (a) at $P_{N_2} = 7$ MPa (1 – 70% Al, 2 – 50% Al, 3 – 40% Al, 4 – 30% Al, 5 – 25% Al, and 6 – 20% Al) and (b) dependence of combustion velocity on relative density of the green mixture at the same Al contents.

incomplete combustion of aluminum. A high content of aluminum was observed in the synthesis products. It can be explained by coalescence of unreacted aluminum and absence of after-burning stage because of remarkable shrinkage of the synthesis products.

1.4
SHS Equipment for Powder Synthesis

The first installation for nitride powder production was a universal SHS equipment including three various hermetic reactors: SHS-30 (30 l capacity), SHS-20 (20 l capacity), and SHS-8.0 (8 l capacity). The SHS-30 reactor is equipped with an automated lock. The reactors can be equipped with the systems controlling the combustion rate and temperature, with personal computer (PC) supervising the parameter changes. They are made of corrosion-resistant refractory steel and can withstand up to 30 MPa. Within carbide or nitride production, this steel is neither carbonized nor nitrided. The temperature on the reactor walls does not exceed 300–500 °C. For laboratory experiments, a reactor of 2.5 l (SHS-2.5) is mainly used.

Development of the universal installation appeared to be an important stage in the development of the technology as it allowed us to synthesize a wide range of refractory compounds and demonstrate a high yield of the technology simultaneously.

The SHS Filtration Combustion (FC) reactor was manufactured for obtaining nitrides under the mode of infiltration combustion. It is distinguished by the oriented gas flow [30], that is, forced infiltration of reactive or impurity gases. Such reactors are equipped with pressure gages and thermal couples, and have pressure-release valves. A grade-up example of the SHS FC reactor is an SHS

reactor for synthesizing nitrides using azides as nitriding substances. This reactor (SHS-Az) belongs to the group of constant pressure installations. The reactor of $5.5-6.5$ l capacity can be used for research; and with the capacity of 19.4 l, it can be used to produce trial lots of nitride and carbonitride ceramic powders [30].

For preliminary preparation of raw materials and final processing of the target products, conventional equipment of powder metallurgy (ball mills, attritors, grinders, and dry kilns) is used. It is desirable to apply up-to-date secondary machinery in order to maintain the technology efficiency and the synthesized product purity [65].

1.5
Synthesis of SHS-Ceramics Based on Silicon and Aluminum Nitrides and SiAlON Powders

Remarkable technological abilities of SHS allowed us to synthesize nitride powders of high quality, with extraordinary structures, high chemical and diffusion activity (in the case of their nonequilibrium state), and excellent characteristics that tell on the items thereof. On the other hand, some "disadvantageous" properties of SHS products such as their poor grindability in comparison with furnace powders and necessity to increase the sintering temperature can worsen the quality of the items unless optimum terms of powder preparation are determined. Nowadays, these difficulties can be overcome by various approaches such as liquid "chemical dispergation" of the powders which allows breaking agglomerates and separating fine nitride particles [43], a decrease in combustion temperature, application of preliminary mechanochemical processing of raw materials, and so on. All these approaches make it possible to widen a range of SHS ceramics and produce materials and items with higher operation characteristics in comparison with their conventional analogs. The examples of the most successfully used materials and items produced from SHS powders at ISMAN and in other institutions are given in this chapter.

1.5.1
Silicon Nitride Powders and Items

Nitride ceramics based on silicon and aluminum nitrides are the most widely used ceramics. One of the first papers describing the production terms and quality of nitride ceramics based on $SHS-Si_3N_4$ with $54-90\%$ of α-phase was published by our Ukrainian colleagues [66]. They studied the influence of two main impurities in Si_3N_4 – iron and oxygen on strength and wear resistance of hot-pressed materials. They determined the material bending strength at $1200\,°C$ with radiation heating in 10^{-3} Pa vacuum as well as its breakdown at friction with pressure using a friction test machine at total loading of $500\,H$ and linear rate of $1\,m\,s^{-1}$. Y_2O_3 (5 mass%) and Al_2O_3 (2 mass%) were used as activating additives. High-dense samples (porosity <3%) were obtained by the method of hot pressing. Some

amount of oxygen and iron was added to the powders to widen the range of investigations. The samples based on Si_3N_4 with 1.5 mass% of oxygen demonstrated high bending strength at the room temperature. Obviously, it is the necessary condition of high-quality sintering and formation of strong structure. Bending strength was weakly dependent on iron content in the powder; at 1200 °C, some material degradation was observed. After analyzing the material wear at friction and load-carrying capacity, the Ukrainian scientists concluded that the optimum mass content of oxygen in the initial powder was ~2.4%. S_3N_4 powder activation by a special technology allowed increasing the material strength 1.5 times. Therefore, the impurity phases of O_2 (SiO_2) and Fe efficiently influence the process of hot pressing of SHS silicon nitride with formation of liquid silicate systems which ensure rearrangement and packing of particles with their subsequent recrystallization and simultaneous $\alpha \to \beta$ transition. Due to that, high dense and strong nitride ceramics were obtained.

Silicon nitride is known to be a promising material for manufacturing friction bearings operating at high and room temperatures. According to the friction coefficient and wear resistance, it can be compared with bronze at lubricated friction of steel, but much better than metal by maximum permissible loadings. The test samples made of SHS-Si_3N_4 [67] contained 75–80% of β-phase, <2% of oxygen, and 0.16% of free silicon. They were sintered in nitrogen medium at 1750 °C during 0.5 h. During tribotechnical tests, the reference sample was made of steel containing 45% of carbon with its hardness being 49–51 Hardness Rockwell scale C (HRC). The slip rate was $1 \, \text{m s}^{-1}$. For each material, the zones of high and optimum power consumption were detected. In the case of 15–20% porosity, the lowest values of wear and friction coefficient were observed. This material is characterized by the highest maximum permissible loading on the friction pair. But sintered silicon nitride is particularly interesting as a high-temperature heat-resistant structural material. Paper [68] demonstrates the data on SHS production of high-quality silicon nitride powder and items thereof with the density of 99% of the theoretical value. The items were obtained by ordinary sintering with introduction of Y_2O_3 (6 mass%) and Al_2O_3 (2–4 mass%) as activating agents. Fracture toughness of the ceramics was $k_{1c} = 5.5–5.6 \, \text{MPa m}^{-1/2}$, microhardness $H_\mu = 17.2–17.9 \, \text{GPa}$. Nowadays, the most interesting are the works on activation of planetary milling combined with introduction of either conventional agents (Y_2O_3, Al_2O_3) or unusual ones, for example, ultradispersed amorphous silicon nitride obtained by SHS with a reduction stage [69]. The authors of this work introduced ~10% of activating agents and sintered the mixture at 1750 °C for 0.5–4 h. The sintered nitride had an optimum structure: β-Si_3N_4 crystals in the matrix of fine equiaxial particles of the same phase and glass (oxide eutectics). Cracking is hardly possible in this case. The material is characterized by high strength properties and heat resistance up to 1200 °C in the air.

There is another approach to obtaining high-quality items from silicon nitride. It implies use of silicon nitride-based powders for sintering with activating agents introduced at the stage of powder production. This approach was widely used in the works by Hizao [70], Pampukh [71], Wang [72], and other scientists.

At synthesis, the agents (Y_2O_3, Al_2O_3) are included in silicon nitride. Uniform distribution of oxides in SHS Si_3N_4 powder and high diffusibility of the solid solution result in a significant increase in its sinterability. At $T_s = 1630\,°C$, the density was ~99%. This approach also allowed suppressing the growth of some grains, and the sintered sample only contained fine ($0.5 - 20\,\mu m$) equiaxial grains.

Homogeneous fine-grained structure is the main target in development of structural materials with high strength at $1300 - 1800\,K$, high hardness, and wear resistance. We carried out some experiments in production of composite materials $Si_3N_4 - Y_2O_3$ and $Si_3N_4 - MgO$ during one stage and their sintering by hot pressing [73]. This approach is very important from the viewpoint of uniform distribution of secondary phases and formation of intergrain phase at the stage of the powder synthesis. The compositions based on α-modification of silicon nitride powder were synthesized in SHS reactors at maximum pressure of 20 MPa. The samples were sintered by hot pressing using induction heating up to $2000 - 2100\,K$ in nitrogen of $P = 15 - 20\,MPa$. The main results of the work were obtained of composite powders of α-$Si_3N_4 - Y_2O_3$ and α-$Si_3N_4 - MgO$ in one stage and determination of the start of α → β phase transition at the temperature lower than the melting point of the corresponding eutectics. Metastable composite powders based on α-Si_3N_4 with high rate of phase transformation were synthesized. When the powders were sintered by hot pressing, the operation characteristics of the obtained ceramics were remarkable: microhardness – up to 26 GPa, crack resistance growth – from $6\,MPa\,m^{1/2}$ at $20\,°C$ up to $10\,MPa\,m^{1/2}$ at $1200\,°C$.

These examples of nitride ceramics based on SHS-Si_3N_4 do not cover all the results obtained by the time. The direction based on application of initial ultradispersed powders for obtaining nanodispersed nitrides is being actively developed. Use of nonequilibrium systems as raw materials is also very promising for improving nitride ceramics quality.

1.5.2
SiAlON Powders and Items

The properties of silicon nitride are close to those of α- and β-SiAlONs which are solid solutions based on silicon nitride, aluminum nitride, and aluminum oxide ($Si_3N_4 - AlN - Al_2O_3$). Elaboration of these systems is one of the promising directions in development of structural ceramics, firstly, because of the unique set of operation characteristics providing application of SiAlON ceramics in various industries. SHS technology of SiAlON production of various compositions is based on infiltration combustion in nitrogen contained in the systems including silicon, aluminum, aluminum oxide, or silicon oxide according to the scheme:

$$(6 - 1.5z)Si + zAl + 0.5zSiO_2 + (4 - 0.5z)N_2 \rightarrow \beta - Si_{6-z}Al_zO_zN_{8-z}. \quad (1.13)$$
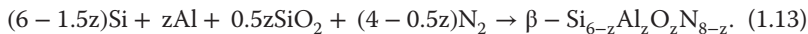
α-SiAlONs doped with rare-earth metals are used as pigments and luminophores. The boundaries of the areas of homogeneous existence of SHS solid solutions correspond to well-known values: $0 \leq z \leq 4.2$ for β-$Si_6 - zAl_zO_zN_{8-z}$ and $0.35 \leq x = 0.9$ for α-$Y_xSi_{12-4.5x}Al_{4.5x}O_{1.5x}N_{16-1.5x}$. The investigations carried

out in several research centers (Spain, Poland, USA, Japan) show that the SHS powders possess excellent sinterability with the temperature $40-70\,°C$ lower than that in the case of the conventional powder use. Their main strength characteristics (bending strength – $600-800\,MPa$, coefficient of fracture toughness – K_{1c} up to $8\,MPa\,m^{0.5}$, microhardness – $16-18\,GPa$) are highly competitive with such characteristics of the best SiAlON ceramics [74]. The efficiency of the sintered SHS-SiAlON as a refractory is demonstrated in [75]. Its stability in stainless steel melt is higher than that of zirconium oxide and aluminum oxide.

Catalytic activity of SiAlON SHS ceramics of various compositions was tested in oxidation reactions of propane, methane, and carbon oxide in gas mixtures modeling the composition of exhaust gas of the internal combustion engine (ICE) [76]. The gas mixture containing CO ($1-10\%$), C_3H_8 ($1-1.5\%$), CH_4 (1%), NO ($0.2-0.44\%$), O_2 ($3-20\%$), and dilutant N_2 was passed through the pipe reactor with SiAlON at $T = 100-750\,°C$. The specific surface area of the SiAlON powder S_{sp} was $26.5\,m^2\,g^{-1}$, of granules – $1.27\,m^2\,g^{-1}$, honeycomb structure blocks – $5\,m^2\,g^{-1}$ with the cell size of $1\times1\,mm$, and wall thickness – $0.1\,mm$. The strength of the blocks was stable up to $1300\,°C$. The SiAlONs demonstrated high catalytic activity, and retained it at work of ICE exhaust gas neutralizer during $1000\,h$ at $150-1000\,°C$. Catalytic activity of SiAlONs containing no noble metals grew when oxide phases of d-metals (Co_3O_4, NiO, Mn_3O_4, etc.) were applied onto their surface. They were tested for complete oxidation of CO and hydrocarbons and for methane oxidation to ethylene [77]. Figure 1.22a,b demonstrates the comparison of activity of SiAlON catalyst with that of the standard catalyst of the type Bead Platinum Catalyst-1. (0.1% of Pt on γ-Al_2O_3). Due to the thorough investigations carried out within this work, we can conclude that SiAlONs are promising carriers which enable us to develop highly efficient catalysts of complete and partial oxidation of CO and hydrocarbons.

(a)   (b)
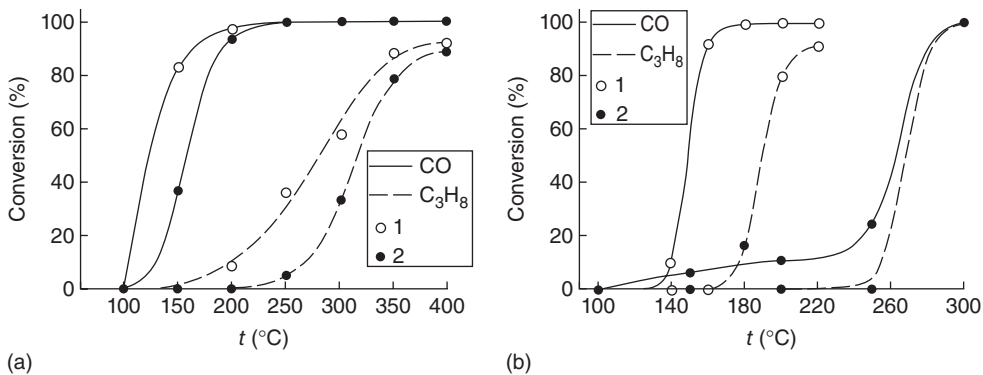
Figure 1.22 Dependence of catalyst activity on temperature at complete oxidation of CO and propane, (a) 1 – Bead Platinum Catalyst-1. ($10\,cm^3$) and 2 – SiAlON $Z = 1$, granules with $2-11\%$ Co_3O_4, $\alpha = 1.3$, $V = 15\,000\,h^{-1}$ and (b) 1 – SiAlON $Z = 3$, fraction $0.1-0.2\,mm$, activated in $Fe(NO_3)_3$ solution, with application of 6.8% Co_3O_4 ($1\,cm^3$) and 2 – Bead Platinum Catalyst-1, fraction $0.1-0.2\,mm$ ($1\,cm^3$), $\alpha = 1.1$, $V = 120\,000\,h^{-1}$.

1.5.3
Aluminum Nitride Powders and Items

Presently, aluminum nitride is considered as an alternative of the items made of toxic and deficit beryllia in many applications. One of the first works that dealt with SHS-AlN application for high dense ceramics is described in [78]. Aluminum nitride powder was synthesized in SHS-8 reactor. The items of AlN were sintered at 1900 °C with the exposure of 1 h. The quality of the sintered materials was controlled by varying open porosity Π_0 and apparent density ρ_k. SHS AlN powders obtained at various parameters (nitrogen pressure, green mixture composition, raw material characteristics, reactive mass density, etc.) were subjected to sintering. The purest aluminum nitride was obtained at P_{N_2} = 10 MPa and dilution of aluminum with nitride (~60 mass%). In all the samples under study, no carbon oxide was detected and free aluminum content was 0.02%. The materials sintered from the aluminum nitride were characterized by minimum porosity 0.12−0.2% and density − 3.29 g cm^{-3}. Specific surface area of AlN was shown to be the main factor determining AlN sinterability at the presence of liquid phase [79]. The latter is amorphous eutectics. It is the result of interaction of activators with aluminum oxynitride film on the nitride particle surface. The dependence of sintered AlN density on the value of the specific surface area looks like "a curve of saturation" (Figure 1.23). SHS powders with prevailing izomorphous round particles with bimodal size distribution were characterized by the best sinterability. The highest value of thermal conductivity of AlN-based ceramics (200−220 W m^{-1} K^{-1}) was achieved in the case of special thermal treatment which resulted in drastic change of the ceramics structure. Complete recrystallization was observed, and new faceted crystals of 15−20 μm in size appeared instead of round particles.
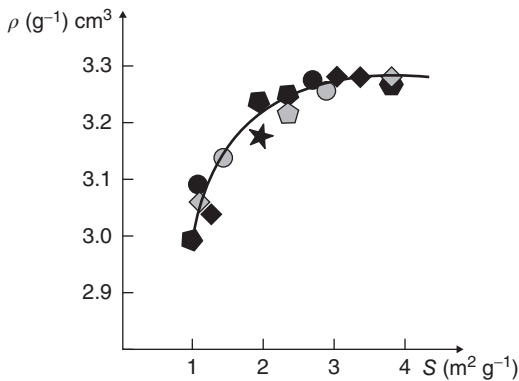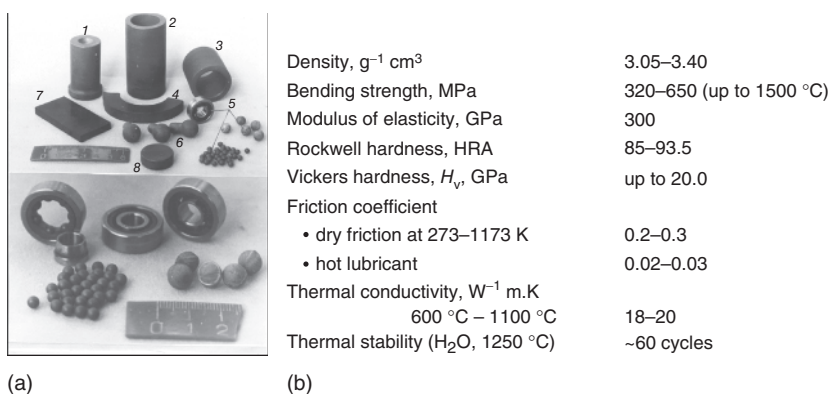

Figure 1.23 Dependence of sinterability of silicon nitride mixtures with yttria on specific surface area.

1.6
Direct Production of Materials and Items Based on Nitride Ceramics by SHS Gasostating

The powder variation of SHS is certainly advantageous. But it supplies only raw materials, which should then be processed by conventional methods of sintering, hot pressing, spraying, and so on. The optimum variation is a combination of SHS with various mechanical and physical actions (pressing, gasostating, and thermal explosion). In this case, both synthesis of a substance with preset chemical and phase composition and formation of the material structure and geometry are carried out simultaneously without a powder preparation stage. In the case of gasostating, the process is carried out in the green mixture preliminarily compacted from solid reagents in the form of the required item or material with the following insignificant machining.

Nitride formation occurs at combustion in nitrogen in the constant pressure reactor under the terms of infiltration combustion. It takes the combustion front a few seconds to propagate along the sample, the temperatures being $2500-3000\,°C$. The SHS gasostats developed at ISMAN allow us to carry out the process at gas pressure of up to 350 MPa [80, 81]. The material or item formation is a complicated process, sometimes with incompatible aims, for example, high initial and low final porosities, retaining of the item geometry and dimensions, and so on. So, some special technological approaches or peculiarities of initial system combustion and state are used in SHS-gasostating. The example of such peculiarities is the so-called volume effect of the nitriding reaction (an increase in a substance weight due to nitrogen capture). This method allowed us to obtain items of the preset size at synthesis of complex "black" ceramics (Si_3N_4-SiC, TiN) [82], Figure 1.24a, and other items of some complicated composition. Some characteristics of "black" ceramics are given in Figure 1.24b. When studying the mechanism of the ceramics formation, we could obtain the material with

Density, $g^{-1}\,cm^3$	3.05–3.40
Bending strength, MPa	320–650 (up to 1500 °C)
Modulus of elasticity, GPa	300
Rockwell hardness, HRA	85–93.5
Vickers hardness, H_v, GPa	up to 20.0
Friction coefficient	
• dry friction at 273–1173 K	0.2–0.3
• hot lubricant	0.02–0.03
Thermal conductivity, $W^{-1}\,m.K$	
600 °C – 1100 °C	18–20
Thermal stability (H_2O, 1250 °C)	~60 cycles

(a)　　　　　　　　　　　　　(b)

Figure 1.24 Synthesis of items with preset size from $Si_3N_4-SiC-TiN(C)$ ceramics (a) and its properties (b).

nanostructured matrix of silicon carbonitride SiC_xN_y hardened by nanoparticles of titanium carbonitride. This material can demonstrate high operation characteristics.

Another important factor in the direct synthesis of ceramic items is volume shrinkage during the combustion process. It is characteristic of the systems containing low-melting components or intermediate products. When used properly, this method makes it possible to synthesize materials and items valuable for practical application.

1.6.1
Nitride Ceramics Based on SiAlONs

The "volume effect" was thoroughly studied at the synthesis of SiAlON ceramics [83, 84]. Figure 1.25 demonstrates the dependence of volume shrinkage (V_0/V_f) on nitrogen pressure for SiAlON–BN ceramics with the combustible component content being 42.5 mass% and initial relative density – $\rho_0 = 0.63$. The ratio of V_0/V_f (initial and final volumes of the sample) constantly grows at the pressure ranging from 30 to 100 MPa, and then it remains practically constant. At the same time, the combustion velocity and rate attain the maximum value ($1-1.6\,\mathrm{mm\,s^{-1}}$, $2300-2600\,\mathrm{K}$) and the surface mode of infiltration combustion transfers to the layer-by-layer type. It allows us to connect the sample shrinkage with deformation processes associated with the reactive gas pressure gradient formation close to the reaction zone. According to the theoretical conception, the pressure gradient has its maximum value and sharp orientation along the combustion axis namely at the layer-by-layer mode.

The optimum use of the volume shrinkage effect gave us an opportunity to carry out the direct synthesis of SiAlON items characterized by high thermal effect
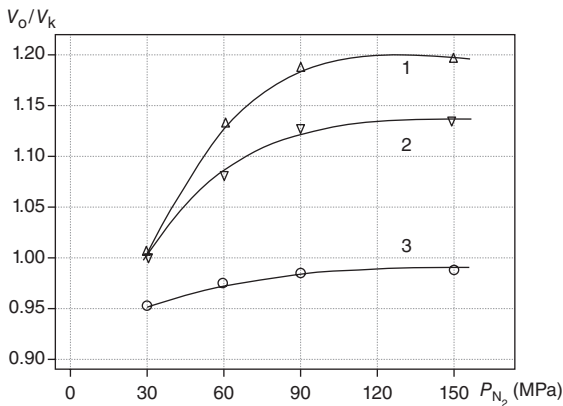
Figure 1.25 Dependence of volume shrinkage of β-$Si_{4.3}Al_{1.7}O_{1.7}N_{0.3}$–BN on nitrogen pressure at combustible component content (%) of 1 – 50, 2 – 42.5, and 3 – 35 (BN – 10%).

Table 1.1 Corrosion wear of ceramic materials in slag and stainless steel melts.

Material under study	Weight loss (mass%)	
	In slag	In stainless steel
ZrO_2-graphite	60	20
Al_2O_3	—	30
ZrO_2	—	50
Si_3N_4	—	17
β-SiAlON	—	5
β-SiAlON$-$SiC$-$BN (SHS)	0	0
Si_3N_4-SiC$-$TiN (SHS)	—	40
BN (SHS)	30	20
BN$-$SiO$_2$ (SHS)	20	20

Slag composition, mass%: SiO_2 29, Al_2O_3 28, CaO 4, Na_2O 6, K_2O 0.5, P_2O_5 0.05, FeO 4, TiO_2 0.3, Cr_2O_3 5, MnO 7. Tested at $T = 1600\,°C$ for 40 min.
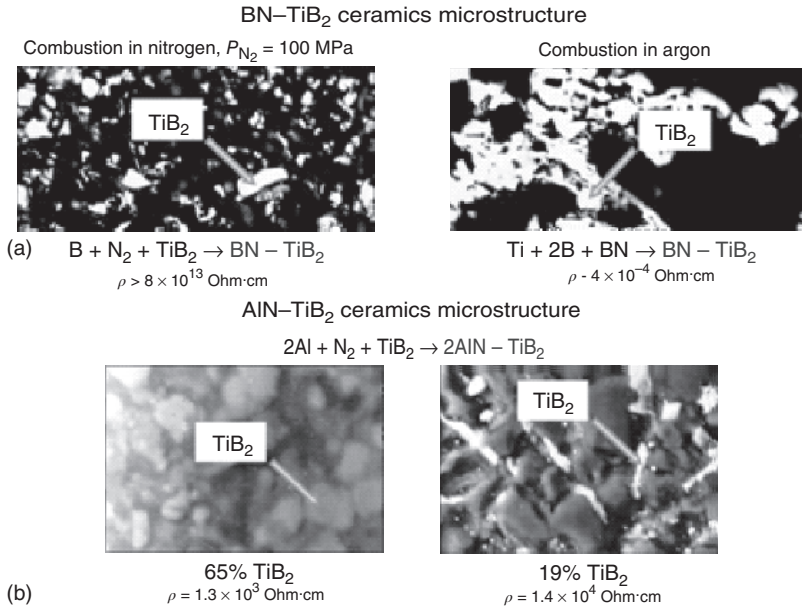
and low corrosion resistance in slag melts or corrosion-resistant steel at $1600\,°C$ (Table 1.1).

A very important peculiarity of SHS gas stating in structure formation of ceramic items with preset properties is the ability of the reagents to develop the frame structures during the combustion process, which are free of impurity clusters decreasing the material operation characteristics. During the investigations, we discovered a new phenomenon – nonuniqueness of binary material structure at the same phase and chemical composition [6, 85]. This phenomenon is described using the example of $BN-TiB_2$, Figure 1.26a,b. Different ways of the reaction realization are shown to result in different structures of $BN-TiB_2$ ceramics. When the mixtures of boron with titanium diboride are nitrided, the material including BN matrix with separate TiB_2 particles is formed. The material is an excellent dielectric (electric conductivity $\rho > 8 \times 10^{13}\,\Omega\,cm$). When SHS proceeds in the system $Ti + 2B + BN$ in the inert medium, a distinct frame structure is formed (TiB_2 paths). The material is characterized by high electric conductivity ($\rho = 4 \times 10^{-4}\,\Omega\,cm$) and used in manufacturing electroconductive evaporative elements for aluminum and other metals evaporation at induction heating. This effect is observed in the cases of other materials based on composite SHS ceramics.

1.6.2
Nitride Ceramics Based on BN

One of the significant directions in SHS is production of nitride ceramics based on BN, as it is an excellent alternative to the conventional method of BN material and item production because of the usual difficulties observed in BN powder sintering. Nowadays, SHS gas-stating method allows us to synthesize directly a wide range

BN–TiB$_2$ ceramics microstructure

Combustion in nitrogen, P_{N_2} = 100 MPa

Combustion in argon

(a) $B + N_2 + TiB_2 \rightarrow BN - TiB_2$

$\rho > 8 \times 10^{13}$ Ohm·cm

$Ti + 2B + BN \rightarrow BN - TiB_2$

$\rho - 4 \times 10^{-4}$ Ohm·cm

AlN–TiB$_2$ ceramics microstructure

$2Al + N_2 + TiB_2 \rightarrow 2AlN - TiB_2$

65% TiB$_2$
$\rho = 1.3 \times 10^3$ Ohm·cm

19% TiB$_2$
$\rho = 1.4 \times 10^4$ Ohm·cm

(b)

Figure 1.26 "Nonuniqueness" of binary material structure at the same phase and chemical composition: (a) BN–TiB$_2$ microstructure and (b) AlN–TiB$_2$ microstructure.

of ceramic materials and items containing BN, Tables 1.2 and 1.3. These items are actively used in various industries, and their operation characteristics are often much better than those of the traditionally obtained items.

Within the theoretical and experimental research, we studied the regularities connecting chemical and phase composition and porosity of the final products with the reactive mixture composition and density, initial combustion temperature, pressure in the reactor, and so on.

BN–SiO$_2$ ceramics appear to be remarkable among the structural materials based on boron nitride. It was obtained by combustion of B–SiO$_2$–N$_2$ and was studied using infrared spectroscopy and X-ray analysis [86]. The obtained data prove that the composite mainly consists of hexagonal boron nitride and

Table 1.2 Operation properties of SHS ceramics.

SHS compound	Refractoriness (°C)	Heat resistance (thermal cycles)	Compression strength (MPa)	Wetting angle at 1600 °C
BN	2000	4	80	100
BN–SiO$_2$	1600	16	80	60
BN–TiB$_2$	2000	6	84	30
SiAlON–SiC–BN	1800	11	>150	25
SiAlON–BN	1600	6	85	25
AlN–TiB$_2$	1800	3	>150	5

Table 1.3 Application of ceramics obtained by direct synthesis.

Ceramics	Items and applications
BN	Molds and crucibles for teeming metal alloys based on iron, cobalt, nickel, chromium, as well as titanium alloys
$BN-TiB_2$	Installations for centrifugal casting "Formaks," "Degudron," and "Minimax"
$BN-SiO_2$	Two to three times increase in operation life
BN_xC_y	Stop valves, crucibles for melting complex alloyed steels, and hardeners
$BN-Al_2O_3$	Teeming machine "Sirius," 50 processes instead of 2–3 (kersil)
$SiAlON-SiC-BN$	Elements of technological installations for growing semiconducting materials, thermal cycling, and so on. Dielectric characteristics are constant; stability is higher than that of quartz, alundum, and graphite
$Si_3N_4-SiC-TiN$	Protection of parts of laser installations; high thermal stability (CO_2-3 kW)
$SiAlON-TiN$	Bushings for air-plasma cutting (instead of Al_2O_3)
TiB_2-B_4C	Cases for measuring temperature of aluminum and other metal melts, $T_{melt} = 790\,°C$, number of cycles – 72 (without destruction) Nozzles for sand- and shot-blasting machines

X-ray-amorphous silicon dioxide. We can assume that at combustion of boron with SiO_2 in nitrogen, BN crystallization occurs with participation of the liquid phase containing boron and nitrogen as well as silicon dioxide. They interfere with SiO_2 crystallization and encourage growth of hexagonal boron nitride crystals. Thorough investigation of the mechanism of $BN-SiO_2$ synthesis allowed us to follow the ways of the combustion product formation and their physical state. Boron solid-phase nitriding was established to start in the warming-up zone. In connection with it, the combustion temperature attains its maximum and exceeds boron melting point [45]. Silicon dioxide also melts in the warming-up zone. In the combustion zone (maximum heat release), maximum growth of the substance volume and a decrease in the sample porosity are observed. In the after-burning zone (volume after nitriding), the temperature decreases. If the residual porosity of the sample remains the same at the level of 25–30%, the conversion degree of boron to nitride increases to the final value ($\eta = 1$), herewith dioxide melt remains. In the crystallization zone, the temperature goes on decreasing, the melt grows hard, and crystal SiO_2 turns to amorphous. At low values of the sample porosity, some side reactions can occur in the reactive mass after the combustion stage with formation of impurity phases: B_2O_3, B_6O, Si, and so on.

1.6.3
Nitride Ceramics Based on AlN

The items based on AlN and its composite materials are also widely used due to its physicochemical characteristics. So, the development of direct synthesis of these materials is an actual task. As it was mentioned above, the main restriction

in the combustion synthesis of nitride-based materials is the insufficient initial concentration of nitrogen in the sample pores. In order to avoid this disadvantage and nitride dissociation, the process is carried out in SHS gasostats at nitrogen pressure of up to 300 MPa. At aluminum nitride synthesis, the initial component was aluminum or its mixtures with aluminum nitride. Some refractory compounds (borides, carbides, oxides, etc.) were introduced into the green mixture to obtain composite materials [87]. A photo of the fracture structure of aluminum nitride obtained from Al + AlN mixture is shown in Figure 1.27; the porosity is 20%. The structure was formed as a result of melting, and the grains of a newly formed aluminum nitride and those of AlN diluent do not differ. Within the combustion process of the mixture of aluminum and titanium diboride, $AlN-TiB_2$ ceramics with various ratios of the components was obtained (Table 1.2). The material density is $\geq 92\%$, Rockwell hardness – $70-80$, and microhardness of TiB_2 grains – $25\,750-31\,800$ MPa and that of AlN matrix – $10\,720-12\,250$ MPa. The material is homogeneous; diboride grains are distributed in the matrix of molten aluminum nitride, and distinct TiB_2 and AlN boundaries are seen.

Several factors – mechanism of liquid aluminum interaction with nitrogen, the second component wettability with the melt, a possibility of chemical interaction between the second component and the melt, the second component capability of melting and the following failure of the components interface – must be taken into account for comprehension of the mechanism of the processes occurring at SHS of aluminum nitride and composites thereof in gasostats. X-ray microanalysis shows that the melt formed in the SHS zone does not interact with titanium diboride; it corresponds to the literature data on the tendency of the wetting angle of titanium diboride with aluminum to 0 and absence of their interaction at the temperatures higher than 1573 K [88]. It is also encouraged by the high melting point of diboride ($T_m = 3223$ K) in comparison with the combustion temperature ($T_c = 2773$ K). Therefore, titanium diboride wettability and its possible melting do not restrain
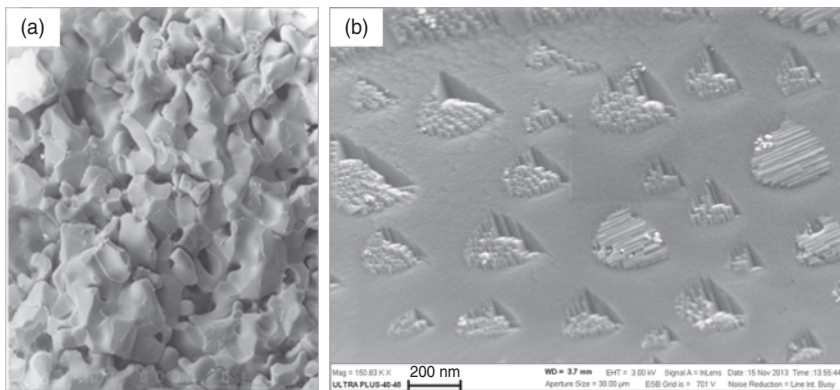
Figure 1.27 Microstructure of molten AlN: (a) fracture surface and (b) microcrystals on matrix surface.

the melt spreading. The existence of molten aluminum nitride matrix and characteristic plateau on heat patterns leads us to confirm that the combustion products are in molten form in the reaction zone. Thorough investigation of the influence of temperature, porosity, shrinkage, and so on, on the product state during SHS proves that the melt of aluminum nitride is formed in the combustion zone. The experimental data allow us to describe the combustion mechanism of aluminum and its mixtures with refractory compounds as the elemental model of the II type – the model of high-temperature melting. But the concept of nonequilibrium mechanism of phase formation should be used too, as it was mentioned above.

The experimental studies of production of boron and aluminum nitride compositions with various refractory compounds by SHS gas-stating prove that the main factors determining the composition of almost all the systems under study and the degree of nitriding are existence of nitriding volume effect, volume shrinkage extent, retaining (or loss) of porosity, and magnitude of the equilibrium wetting angle. The synthesis peculiarities inherent for each specific system are connected with physicochemical properties of refractory compounds making the composition with nitrides of boron, aluminum, and other elements.

1.7
Conclusion

While putting the finishing touch in this chapter, we would like to underline that it was nitrides and composites thereof that played a significant role in the development of SHS R&D and contributed greatly to a better comprehension of the processes occurring at combustion synthesis and regularities of product phase and structure formation. Investigation of nitride formation mechanism and peculiarities at combustion encouraged the origin of such a scientific field as structural macrokinetics. Theoretical studies carried out by the scientists from ISMAN: Merzhanov, Aldushin, Shkadinsky, Seplyarsky, Grachev, Ivleva, and their colleagues from different Russian institutes and abroad appeared to be remarkable in the development of this field. An important contribution was made by the researchers headed by Maksimov from Tomsk, who elaborated theoretical and practical backgrounds of metal and alloy nitriding at combustion, and their colleagues headed by Amosov from Samara, who developed the azide variation of SHS.

References

1. Merzhanov, A. and Borovinskaya, I. (1972) *Dokl. Akad. Nauk SSSR*, **204** (2), 366–369.
2. Merzhanov, A. and Borovinskaya, I. (1975) *Combust. Sci. Technol.*, **10** (5–6), 195–200.
3. Merzhanov, A. (1990) in *Combustion and Plasma Synthesis of High-Temperature Materials* (eds Z.A. Munir and J.B. Holt), VCH Publisher, New York, pp. 1–53.

4. Borovinskaya, I. (1992) *Pure Appl. Chem.*, **64** (7), 919–940.

5. Munir, Z. and Anselmi-Tamburini, U. (1989) *Mater. Sci. Reports*, **3** (7–8), 277–365.

6. (a) Merzhanov, A., Borovinskaya, I., *Int. J. SHS*, 2008, 17(4), 242-265; (b) Merzhanov, A., Borovinskaya, I., Forum WAC: Ceramic Materials in Energy Systems for Sustainable Development, Chianciano Terme, 2008.

7. Hagg, G. (1931) *Z. Phys. Chem.*, **12**, 33.

8. Borovinskaya, I. (1972) Self-propagating High-temperature Synthesis of Nitrides. PhD Thesis, Chernogolovka.

9. Borovinskaya, I. and Loryan, V. (1976) *Dokl. Akad. Nauk SSSR*, **231** (4), 911–914.

10. Borovinskaya, I. and Loryan, V. (1978) *Poroshkovaya Metall.*, **11** (191), 42–45.

11. Merzhanov, A. and Rumanov, E. (1977) *Izvestiya AN SSSR, Met.*, **3**, 188–193.

12. Merzhanov, A., Filonenko, A., and Borovinskaya, I. (1973) *Dokl. AN SSSR*, **208** (4), 892–894.

13. Munir, Z. and Holt, J. (1987) *J. Mater. Sci.*, **22**, 710–714.

14. Borovinskaya, I. (1977) *Gorenie i Vzryv, IV Symposium on Combustion*, Nauka, Moscow, pp. 138–148.

15. Borovinskaya, I., Merzhanov, A., Pityulin, A., and Shehtman, V. (1975) in *Combustion Processes in Chemical Technology and Metallurgy* (ed. A.G. Merzhanov), USSR Academy of Science, Chernogolovka, p. 133.

16. Borovinskaya, I., Merzhanov, A., and Pityulin, A. (1975) *Combustion Processes in Chemical Technology and Metallurgy*, Publishing department of The Branch of Institute for Chemical Physics, Russian Academy of Sciences, Chernogolovka, pp. 113–118.

17. Vidavsky, Y. and Konovalov, S. (1983) *J. Inorg. Chem.*, 2412–2414.

18. Itin, V., Bratchykov, A., Doronin, V., and Pribitkov, G. (1981) *Izv. Vuzov, Fiz.*, **12**, 75–78.

19. Boldyrev, V., Aleksandrov, V., and Korchagin, M.A. (1981) *Dokl. Akad. Nauk SSSR*, **5**, 1127–1129.

20. Frahm, R., Wong, J., Holt, J., Larson, E., Rupp, B., and Waide, A. (1992) *AIP Conf. Proc.*, **258**, 615–620.

21. Knyazik, V., Merzhanov, A., Solomonov, V., and Shteinberg, A. (1985) *Fiz. Goreniya Vzryva*, **3**, 69.

22. Loryan, V. (1995) Self-propagating High-temperature Synthesis of Nitride Ceramics at High Pressure of Nitrogen. D.Sci. Thesis, Chernogolovka.

23. Borovinskaya, I., Veshnyakova, G., and Loryan, V. (1991) *Problems of Structural Macrokinetics*, Publishing department of Institute of Structural Macrokinetics, Russian Academy of Sciences, Chernogolovka, pp. 5–21.

24. Hirao, K., Miyamoto, Y., and Koizumi, M. (1987) *J. Soc. Mater. Sci.*, **36** (400), 12.

25. Munir, Z. and Anselmi-Tamburini, U. (1989) *Mater Sci. Rep.*, **3** (7–8), 277–365.

26. Khidirov, I., Karimov, I., Em, V., Loryan, V., and Borovinskaya, I. (1980) *Dokl. Akad. Nauk SSSR*, **195**, 29–31.

27. Khidirov, I., Karimov, I., Em, V.T., and Loryan, T. (1986) *Izv. AN SSSR*, **22** (10), 1675–1678.

28. (a) Merzhanov, A. (2000) *Solid Flame Combustion*, Publishing department of Institute of Structural Macrokinetics, Russian Academy of Sciences, Chernogolovka, p. 238; (b) Merzhanov, A. and Mukasyan, A. (2007) *Solid Flame Combustion*, 2nd edn, Torus Press, Moscow, p. 336.

29. Mamyan, S. and Vershinnikov, V. (1992) *Int. J. SHS*, **1** (3), 392–400.

30. (a) Amosov, A., Borovinskaya, I., and Merzhanov, A. (2007) *Powder Technology of Self-propagating High-temperature Synthesis of Materials*, Mashinostroenie, Moscow, p. 567; (b) Amosov, A., Bichurov, N., and Bolshova, V. (1992) *Int. J. SHS*, **1** (2), 239–245.

31. Mukasyan, A. and Borovinskaya, I. (1992) *Int. J. SHS*, **1** (1), 55–63.

32. Mukasyan, A., Martynenko, V., Merzhanov, A., Dorovinskaya, I., and Blinov, M. (1986) *Fiz. Goreniya Vzryva*, **5**, 43–49.

33. Cano, J., Borovinskaya, I., Rodriguez, A., and Grachev, V. (2002) *J. Am. Ceram. Soc.*, **85** (9), 2209–2211.

34. Zakorzhevsky, V. (2004) Self-propagating High-temperature Synthesis of Silicon

Nitride, Aluminum Nitride and Composite Powders Based on these Nitrides. PhD Thesis, Chernogolovka.

35. Merzhanov, A., Borovinskaya, I., Khomenko, I., Mukasyan, A., Ponomarev, V., Rogachev, A., and Shkiro, V. (1995) *Ann. Chim. Fr.*, **20**, 123–138.

36. Merzhanov, A., Borovinskaya, I., and Loryn, V. (2011) *Abstracts. XIX Mendeleev Forum on General and Applied Chemistry*, Publishing department of Volgograd State Technical University, Volgograd, p. 76, 536, 600, 704.

37. (a) Sytchev, A. and Merzhanov, A. (2004) *Usp. Khim.*, **73** (2), 157; (b) Sytchev, A. and Merzhanov, A. (2004) *Russ. Chem. Rev.*, **73** (2), 147–159.

38. Suslik, K. and Price, G. (2010) in *Nanotechnology* (ed. Y.D. Tretyakov), Fizmatlit, Moscow, p. 368.

39. Andrievsky, R. and Ragulya, A. (2005) *Nanostructural Materials*, Academic Press, Moscow, p. 193.

40. Borovinskaya, I. (2012) Abstracts. XI International Symposium on SHS, 2011, Attica, Greece, p. 75.

41. Mukasyan, A., Stepanov, B., Galchenko, Y., and Borovinskaya, I. (1990) *Fiz. Goreniya Vzryva*, **1**, 104–108.

42. Melikhov, I. (2006) *Physico-chemical Evolution of Solids*, Binom, Moscow, p. 309.

43. Borovinskaya, I., Ignat'eva, T., Vershinnikov, V., Khurtina, G., and Sachkova, N. (2003) *Neorg. Mater.*, **39** (6), 698–704.

44. Loryan, V., Borovinskaya, I., and Merzhanov, A. (2009) *Int. J. SHS*, **18**, 154–156.

45. Loryan, V., Borovinskaya, I., and Merzhanov, A. (2011) *Int. J. SHS*, **20** (3), 153–155.

46. Pirtskhalaishvili, R., Bayramishvili, I., Samkurashvili, T., Lomidze, G., Loladze, S., and Gudushauri, N. (1974) *Boron, Production, Structure, Properties*, Science, Moscow, pp. 23–26.

47. Borovinskaya, I. (1974) *Archiwum Procesow Spalania*, **5**, 145–161.

48. Borovinskaya, I., Merzhanov, A., Dubovitsky, F., and Enman, V. (1970) Certificate USSR, No. 1393281/23-26, 1970.

49. Zakorzhevsky, V., Borovinskaya, I., and Sachkova, N. (2002) *Neorg. Mater.*, **38** (11), 109–115.

50. Zakorzhevsky, V. and Borovinskaya, I. (2011) *Int. J. SHS*, **20** (3), 154–158.

51. Merzhanov, A., Borovinskaya, I., and Volodin, Y. (1972) *Dokl. AN SSSR*, **206** (4), 905–908.

52. Aldushin, A., Merzhanov, A., and Khaikin, B. (1974) *Dokl. AN SSSR*, **315** (3), 612–615.

53. Grachev, V. and Borovinskaya, I. (2006) *Adv. Sci. Technol.*, **45**, 1011–1017.

54. Borovinskaya, I., Merzhanov, A., Mukasyan, A., Rogachev, A., Khina, B., and Khusid, B. (1992) *Dokl. AN SSSR, Phys.Chem.*, **322** (5), 912–917.

55. Grachev, V., Ivleva, T., Borovinskaya, I., and Merzhanov, A. (1996) *Dokl. AN SSSR, Chem.*, **346** (5), 626–629.

56. Borovinskaya, I., Merzhanov, A., Butakov, A., Ryabinkin, A., and Shehtman, V. Method of producing Tantalum Nitride. (1970) Patent SU 264365, Bull. invent., 1970, 9.

57. Molodovskaya, E., Petrunin, V., Karimov, I., Kalanov, M., Khaidarov, T., Borovinskaya, I., Pityulin, A., and Merzhanov, A. (1975) *Fiz. Met. Metalloved. Akad. Nauk SSSR*, **40**, 202–204.

58. Borovinskaya, I. and Pityulin, A. (1978) *Fiz. Goreniya Vzryva*, **1**, 137–140.

59. Merzhanov, A. (1995) *Int. J. SHS*, **4** (4), 323–350.

60. Merzhanov, A., Rogachev, A., Mukasyan, A., and Khusid, B. (1990) *Fiz. Goreniya Vzryva*, **1**, 104–114.

61. Merzhanov, A. and Rogachev, A. (1992) *Pure Appl. Chem.*, **64** (7), 941–953.

62. Andrievsky, R. and Lyutikov, R. (1996) *Zh. Fiz. Khim.*, **70** (3), 567–569.

63. Ivleva, T., Merzhanov, A., and Shkadinsky, G. (1980) *Fiz. Goreniya Vzryva*, **16** (2), 3–10.

64. Zakorzhevsky, V. and Borovinskaya, I. (2002) *Inorg. Mater.*, **38** (11), 1140.

65. Martirosyan, H., Dolukhanyan, S., Mkrtchyan, G., Borovinskaya, I., and Merzhanov, A. (1977) *Poroshkovaya Metall.*, 7.

66. Osipova, I., Borovinskaya, I., and Yaroshenko, V. (1996) *Poroshkovaya Metall.*, **1/2**, 98–102.

67. Sharivker, S. and Borovinskaya, I. (1995) *Mashinostroitel*, **9**, 20–23.

68. Sharivker, S. (1995) *Ann. Chem. Phys.*, **20**, 157–167.

69. Sharivker, S., Mamyan, S., Vlasov, V., and Mukasyan, A. (1994) *Poroshkovaya Metall.*, **9/10**, 107–111.

70. Hizao, K., Miyamoto, Y., and Koizumi, M. (1987) *J. Ceram. Soc. Jpn.*, **95** (10), 955–960.

71. Pampuch, R. (1997) *Int. J. SHS*, **6** (2), 187–201.

72. Wang, L., Sigmund, W., Roy, S., and Aldinger, F. (1999) *J. Mater. Res.*, **14** (12), 1456–1459.

73. Zakorzhevsky, V., Borovinskaya, I., Chevykalova, L., and Kelina, I. (2007) *Poroshkovaya Metall.*, **1/2**, 10–14.

74. Loryan, V., Borovinskaya, I., Smirnov, K., and Titov, S. (2012) *Int. J. SHS*, **21** (1), 41–44.

75. Levashov, E., Filonov, M., and Borovinskaya, I. (1995) *J. Mater. Synth. Process.*, **3** (2), 111–114.

76. Borovinskaya, I., Loryan, V., Grigoryan, E., Salnikova, E., and Pershikova, N. (1992) *Int. J. SHS*, **1** (1), 131–134.

77. Borshch, V., Zhuk, S., Vakin, N., Smirnov, K., Borovinskaya, I., and Merzhanov, A. (2008) *Dokl. AN SSSR*, **420** (4), 496–499.

78. Prokudina, V., Shestakova, T., Borovinskaya, I., Kuznetsova, I., Gracheva, N., and Nedelko, E. (1981) *Problems of Technological Combustion*, vol. 2, Publishing department of The Branch of Institute for Chemical Physics, Russian Academy of Sciences, Chernogolovka, pp. 5–8.

79. Zakorzhevsky, V., Sharivker, S., Borovinskaya, I., Ignatieva, T., and Sachkova, N. (1999) *Int. J. SHS*, **8** (2), 165–176.

80. Borovinskaya, I., Loryan, E., Kudakhtin, V., Losikov, A., Merzhanov, A., Ratnikov, V., and Shekk, G. (1993) Installation for producing of compact items from nitride ceramics in the regime of combustion. Patent RU 1780241, Bull. Izobretenii of 27.09.1995.

81. Ratnikov, V., Borovinskaya, I., and Prokudina, V. (2013) *Izvestiya Vuzov, Poroshkovaya Metall.*, **1**, 34–41.

82. Borovinskaya, I., Loryan, V., Blinov, M., and Zozulya, V. (1991) *Ogneupory*, **9**, 15–17.

83. Borovinskaya, I. and Smirnov, K. (1998) *Nauka Proizvodstvu*, **8** (10), 70–74.

84. Borovinskaya, I. and Smirnov, K. (2001) *Key Eng. Mater.*, **217**, 159–164.

85. Borovinskaya, I. (2007) Presentation at XVIII Mendeleev Forum on General and Applied Chemistry, Moscow, 2007.

86. Shulga, Y. and Loryan, V. (1994) *Zhurn. Neorg. Khim.*, **39** (7), 1096–1099.

87. Loryan, V. and Borovinskaya, I. (2003) *Combust. Explos. Shock Waves*, **39** (5), 525–533.

88. Yasinskaya, G. (1966) *Poroshkovaya Metall.*, **7**, 53–56.